DOI:
10.1016/j.mrfmmm.2015.01.013

Document Version
Peer reviewed version

TP53 mutations induced by BPDE in Xpa-WT and Xpa-Null human *TP53* knock-in (Hupki) mouse embryo fibroblasts

Jill E. Kucab[1], Harry van Steeg[2], Mirjam Luijten[2], Heinz H. Schmeiser[3], Paul A. White[4], David H. Phillips[1] and Volker M. Arlt[1]

[1]*Analytical and Environmental Sciences Division, MRC-PHE Centre for Environment & Health, King's College London, London SE1 9NH, United Kingdom*

[2]*Center for Health Protection, National Institute for Public Health and the Environment (RIVM), Bilthoven 3721 MA, The Netherlands*

[3]*Radiopharmaceutical Chemistry E030, German Cancer Research Center (DKFZ), Im Neuenheimer Feld 280, 69120 Heidelberg, Germany*

[4]*Environmental Health Science and Research Bureau, Health Canada, 50 Colombine Driveway, Ottawa, Ontario K1A 0K9, Canada*

Correspondence to: Jill E. Kucab, Analytical and Environmental Sciences Division, MRC-PHE Centre for Environment & Health, King's College London, Franklin-Wilkins Building, 150 Stamford Street, London SE1 9NH, United Kingdom, Tel: +44-207-848-3781, E-mail: jill.kucab@kcl.ac.uk

Abstract

Somatic mutations in the tumour suppressor gene *TP53* occur in more than 50% of human tumours; in some instances exposure to environmental carcinogens can be linked to characteristic mutational signatures. The Hupki (human *TP53* knock-in) mouse embryo fibroblast (HUF) immortalisation assay (HIMA) is a useful model for studying the impact of environmental carcinogens on *TP53* mutagenesis. In an effort to increase the frequency of *TP53*-mutated clones achievable in the HIMA, we generated nucleotide excision repair (NER)-deficient HUFs by crossing the Hupki mouse with an *Xpa*-knockout (Xpa-Null) mouse. We hypothesized that carcinogen-induced DNA adducts would persist in the *TP53* sequence of Xpa-Null HUFs leading to an increased propensity for mismatched base pairing and mutation during replication of adducted DNA. We found that Xpa-Null Hupki mice, and HUFs derived from them, were more sensitive to the environmental carcinogen benzo[*a*]pyrene (BaP) than their wild-type (Xpa-WT) counterparts. Following treatment with the reactive metabolite of BaP, benzo[*a*]pyrene-7,8-diol-9,10-epoxide (BPDE), Xpa-WT and Xpa-Null HUF cultures were subjected to the HIMA. A significant increase in *TP53* mutations on the transcribed strand was detected in Xpa-Null HUFs compared to Xpa-WT HUFs, but the *TP53*-mutant frequency overall was not significantly different between the two genotypes. BPDE induced mutations primarily at G:C base pairs, with approximately half occurring at CpG sites, and the predominant mutation type was G:C>T:A in both Xpa-WT and Xpa-Null cells. Further, several of the *TP53* mutation hotspots identified in smokers' lung cancer were mutated by BPDE in HUFs (codons 157, 158, 245, 248, 249, 273). Therefore, the pattern and spectrum of BPDE-induced *TP53* mutations in the HIMA are consistent with *TP53* mutations detected in lung tumours of smokers. While Xpa-Null HUFs exhibited increased sensitivity to BPDE-induced damage on the transcribed strand, NER-deficiency did not enhance *TP53* mutagenesis resulting from damage on the non-transcribed strand in this model.

1. Introduction

The tumour suppressor p53 plays a crucial role in the DNA damage response, garnering the title 'guardian of the genome' [1]. A paramount function of p53 is to prevent DNA synthesis and cell division, or to promote apoptosis, following DNA damage, which it performs primarily by regulating a large network of transcriptional targets [2, 3]. Disruption of the normal p53 response by *TP53* mutation contributes to transformation by eliminating a key pathway of cellular growth control, enabling the survival and proliferation of stressed or damaged cells. Somatic mutations in *TP53* occur in more than 50% of human cancers [4, 5]. The majority of *TP53* mutations are missense and occur between codons 125 and 300, corresponding to the coding region for the DNA binding domain [6]. Over 28,000 *TP53* mutations from human tumours have been catalogued in the International Agency for Research on Cancer (IARC) TP53 mutation database, providing a key resource for studying the patterns and frequencies of these mutations in cancer [7]. Interestingly, exposure to some environmental carcinogens can be linked to characteristic signatures of mutations in *TP53*, which provide molecular clues to the aetiology of human tumours [8].

A useful model for studying human *TP53* mutagenesis is the partial human *TP53* knock-in (Hupki) mouse, in which exons 4-9 of human *TP53* replace the corresponding mouse exons [9]. The Hupki mouse and Hupki mouse embryo fibroblasts (HUFs) have been used for both *in vivo* and *in vitro* studies of *TP53* mutations induced by environmental carcinogens [10, 11]. *TP53* mutagenesis can be studied in cell culture using the HUF immortalisation assay (HIMA). In this assay primary HUFs are first treated with a mutagen to induce mutations. The treated cultures, along with untreated control cultures, are then serially passaged under standard culture conditions, whereby the majority of HUFs will undergo p53-dependent senescent growth arrest, due to the sensitivity of mouse cells to atmospheric oxygen levels (20%). HUFs that have accumulated mutagen-induced or spontaneous mutations (*e.g.* in *TP53*) that enable bypass of senescence continue to proliferate and ultimately become established into immortalised cell lines. DNA from immortalised HUF clones is then sequenced to identify *TP53* mutations. Environmental carcinogens that have been examined using the HIMA include ultraviolet (UV) radiation [12], benzo[*a*]pyrene (BaP) [13, 14] and aristolochic acid I (AAI) [12, 15]; in all cases the induced *TP53* mutation pattern corresponded to the pattern found in human tumours from patients exposed to these mutagens.

To protect the genome from mutation, several efficient mechanisms exist in cells to repair damage to DNA. One key repair system responsible for removing damage induced by certain environmental carcinogens is the nucleotide excision repair (NER) pathway. NER removes several types of structurally distinct DNA lesions including UV-induced photolesions, intrastrand crosslinks and chemically-induced bulky DNA adducts, such as those formed after exposure to polycyclic aromatic hydrocarbons (PAHs) [16]. NER operates in two distinct subpathways: global

genomic NER (GG-NER) that recognises lesions that cause local structural distortions in the genome, and transcription-coupled NER (TC-NER) that responds to lesions that block the progression of RNA polymerase II (RNAPII) on the transcribed strand of transcriptionally active genes. Following damage recognition, a common set of factors are recruited that ultimately incise the DNA 5' and 3' to the lesion to remove a 24-32 nucleotide fragment. The undamaged strand serves as a template for replicative DNA polymerases to fill the gap, which is finally sealed by ligation [17].

Mouse models deficient in various NER components have been generated not only to study the role of NER in the repair of different types of damage and ascertain how this relates to cancer risk [18, 19], but also to increase the sensitivity of carcinogenicity studies [20]. For example, *Xpa*-knockout (Xpa-Null) mice, or cells derived from them, are deficient in both GG-NER and TC-NER. Xpa-Null mice are highly sensitive to environmental carcinogens [18, 21] and exhibit accelerated and enhanced tumour formation after treatment with carcinogens such as UV and PAHs like BaP, compared with wild-type (Xpa-WT) mice [19, 22, 23]. Increased mutation frequencies of a *lacZ* reporter gene have been measured in tissues from Xpa-Null mice treated with the aforementioned carcinogens, and an increased rate of p53-mutated foci was detected on the skin of Xpa-Null *Trp53(+/-)* mice exposed to UVB [21, 22, 24]. Further, in *in vitro* studies, cells with reduced or deficient repair capacity were also more sensitive to the lethal or mutagenic effects of DNA damage [18, 25, 26].

Here we have generated an *Xpa*-deficient Hupki mouse strain with the aim of increasing *TP53* mutation frequency in the HIMA. As Xpa-Null cells are completely deficient in NER, we hypothesized that carcinogen-induced DNA adducts would persist in the *TP53* sequence of Xpa-Null HUFs, leading to an increased propensity for mismatched base pairing and mutation during replication of adducted DNA [24, 27]. In the present study primary Xpa-WT and Xpa-Null HUFs were treated with benzo[*a*]pyrene-7,8-diol-9,10-epoxide (BPDE), the activated metabolite of the human carcinogen BaP [28, 29], which forms pre-mutagenic BPDE-DNA adducts (*i.e.* 10-(deoxyguanosin-N^2-yl)-7,8,9-trihydroxy-7,8,9,10-tetrahydrobenzo[*a*]pyrene [BPDE-N^2-dG]) that can be removed by NER (**Fig. S1**) [30]. BPDE-treated HUFs were subjected to the HIMA and *TP53* mutations in immortalised clones were identified by direct dideoxy sequencing of exons 4-9. The induced *TP53* mutation patterns and spectra were compared between the two *Xpa* genotypes and to mutations found in human tumours.

2. Materials and Methods

2.1. Carcinogens

BaP (#B1760) was purchased from Sigma-Aldrich. For *in vitro* treatments, BaP was dissolved in DMSO (Sigma #D2650) to a stock concentration of 1 mM and stored at –20°C. For *in vivo* treatments, BaP was dissolved in corn oil at a concentration of 12.5 mg/mL. BPDE was synthesised at the Institute of Cancer Research (London, UK) using a previously published method [31]. BPDE was dissolved in DMSO to a stock concentration of 2 mM under argon gas and stored at –80°C in single-use aliquots.

2.2. Details of mouse strains and crossbreeding

Hupki mice (Trp53$^{tm1/Holl}$ (Arg/Arg codon 72), homozygous for a knock-in *TP53* allele harbouring the wild-type human *TP53* DNA sequence spanning exons 4–9) in the 129/Sv background [9] were kindly provided by Monica Hollstein (German Cancer Research Center; Heidelberg, Germany). Transgenic *Xpa*$^{+/-}$ mice, heterozygous for the *Xpa*-knockout allele on a C57Bl/6 background [18, 22] were obtained from the National Institute for Public Health and the Environment (Bilthoven, The Netherlands). In the *Xpa*-knockout allele, exon 3, intron 3 and exon 4 have been replaced by a neomycin resistance cassette with a PGK2 promoter. To generate Hupki mice carrying an *Xpa*-knockout allele, *Hupki*$^{+/+}$ mice were first crossed with *Xpa*$^{+/-}$ mice. Progeny with the *Hupki*$^{+/-}$*;Xpa*$^{+/-}$ genotype were then backcrossed to *Hupki*$^{+/+}$ stock to generate *Hupki*$^{+/+}$ animals that were *Xpa*$^{+/+}$ or *Xpa*$^{+/-}$. *Hupki*$^{+/+}$*;Xpa*$^{+/-}$ and *Hupki*$^{+/+}$*;Xpa*$^{+/+}$ offspring were thereafter intercrossed to maintain the colony and produce *Xpa*$^{+/+}$ and *Xpa*$^{-/-}$ (referred to here as Xpa-WT and Xpa-Null, respectively) mice and embryos for experiments. Animals were bred at the Institute of Cancer Research in Sutton, UK and kept under standard conditions with food and water *ad libitum*. All animal procedures were carried out under license in accordance with the law and following local ethical review.

2.3. Genotyping

The *Hupki* and *Xpa* genotype was determined in mouse pups or embryos by PCR prior to experiments. To extract DNA for genotyping, ear clips or cells were suspended in 400 µL of 50 mM NaOH and heated to 95°C for 15 min. Next, 35 µL of 1 M Tris-HCl (pH 8.0) was added to each sample, followed by centrifugation for 20 min at 13,000 rpm. The supernatant was used for genotyping. Primers and PCR reaction conditions for the *Hupki*, mouse *Trp53* or *Xpa* alleles are described in **Table S1**.

2.4. In-vivo carcinogen treatment

Female Xpa-WT and Xpa-Null Hupki mice (~3 months old) were treated with BaP as indicated below and sacrificed either 24 hr or 5 days after the last administration following treatment regimens published previously [28, 32]. Several organs (liver, lung, small intestine, spleen, colon and kidney) were removed, snap frozen in liquid N_2, and stored at −80°C until analysis.

In the first experiment, three groups of animals (n = 3, each group) were treated orally with 125 mg/kg bw of BaP. Groups 1 and 2 received a single dose and Group 3 was dosed once daily for 5 days. Groups 1 and 3 were sacrificed 24 hr after the last administration, and Group 2 was sacrificed 5 days after the last administration. In the second experiment, two groups of animals (Group 4 and 5; n = 3, each group) were treated with 12.5 mg/kg bw BaP. Group 4 was treated with a single dose and sacrificed 24 hr later. Group 5 was dosed once daily for 5 days and sacrificed 24 hr after the last administration. Matched control mice (n = 3) for each group received corn oil only. DNA adduct formation was assessed as described below.

2.5. DNA adduct analysis by ^{32}P-postlabelling

Genomic DNA was isolated from cells or tissue by a standard phenol/chloroform extraction method and stored at –20°C. DNA adducts were measured in each DNA sample using the nuclease P1 enrichment version of the ^{32}P-postlabelling method [33]. Briefly, DNA samples (4 μg) were digested with micrococcal nuclease (120 mU; Sigma, #N3755) and calf spleen phosphodiesterase (40 mU; Calbiochem, #524711), enriched and labelled as reported [28, 34]. Solvent conditions for the resolution of ^{32}P-labelled adducts on polyethyleneimine-cellulose (PEI) thin-layer chromatography (TLC) were: D1, 1.0 M sodium phosphate, pH 6; D3, 4.0 M lithium-formate, 7.0 M urea, pH 3.5; D4, 0.8 M lithium chloride, 0.5 M Tris, 8.5 M urea, pH 8. After chromatography TLC plates were scanned using a Packard Instant Imager (Dowers Grove, IL, USA). DNA adduct levels (RAL, relative adduct labelling) were calculated from adduct counts per minute (cpm), the specific activity of [γ-^{32}P]ATP (Hartmann Analytic #HP601ND) and the amount of DNA (pmol) used. Results were expressed as DNA adducts/10^8 normal nucleotides (nt). An external BPDE-modified DNA standard was used for identification of BaP-DNA adducts.

2.6. Isolation of primary mouse embryonic fibroblasts

Xpa-WT and Xpa-Null Hupki mouse embryonic fibroblasts (HUFs) were isolated from day 13.5 embryos of intercrosses of *Hupki*$^{+/+}$*;Xpa*$^{+/-}$ mice according to a standard procedure. Briefly, neural and haematopoietic tissues were removed from each embryo by dissection and the remaining tissue was digested in 1 mL of 0.05% trypsin-EDTA (Invitrogen #25300-062) at 37°C for 30 min. The resulting cell suspension from each embryo was mixed with 9 mL of growth medium

(Dulbecco's modified medium (Invitrogen #31966-021) supplemented with 10% fetal bovine serum (Invitrogen #26140-079) and 100 U/mL penicillin and streptomycin (Invitrogen #15140-130)), pelleted at 1000 rpm for 5 min, and then transferred into a 175-cm^2 tissue-culture flask containing 35 mL of growth medium. Cells were cultured to 80-90% confluence at 37°C/5% CO_2/3% O_2 before preparing frozen stocks (passage 0; approximately 3 days). Fibroblast cultures were genotyped as described above.

2.7. Culture of HUFs and growth curves

HUFs were cultured in growth medium (see 2.6) at 37°C/5% CO_2 with either 20% or 3% O_2, adjusted using an incubator fitted with an oxygen sensor and a nitrogen source. All manipulations conducted outside the incubator were performed at 20% O_2. For passaging, cells were detached with 0.05% trypsin-EDTA for 2–3 min, suspended in growth media and reseeded at the desired cell number or dilution. When required, cells were counted using an Improved Neubauer Hemacytometer according to the manufacturer's instructions.

Mammalian cell culture, including that of HUFs, typically takes place in incubators containing ambient air buffered with 5–10% CO_2, which contains a much higher level of oxygen (20%) than the concentration to which tissues are exposed *in vivo*. The mean tissue level of oxygen is variable, but is typically about 3%, and mean oxygen tension in an embryo may be even less [35]. Mouse cells are more sensitive than human cells to growth at 20% O_2, whereby they accumulate more DNA damage and respond by entering senescence within two weeks of culture [36, 37]. While this is required for the selective growth of *TP53*-mutated clones in the HIMA, it also limits the number of primary cells available for experiments prior to initiating an assay (*e.g.* optimising carcinogen treatment conditions). It was shown previously that culture-induced senescence of primary mouse embryo fibroblasts (MEFs) could be inhibited by growing cells in 3% (physiological) oxygen [37].

To compare the growth of HUFs at atmospheric or physiological oxygen levels, passage 0 primary HUFs (Xpa-WT and Xpa-Null) were thawed and cultured in either 20% O_2 or 3% O_2. After 48 hr, the cells were trypsinised and counted. Cells (2.5×10^5) were reseeded into 25-cm^2 flasks and again incubated at either 20% or 3% O_2. Cells were counted every 3–4 days and reseeded at 2.5×10^5 cells/25-cm^2 flask for several weeks. Cultures in 3% O_2 began to proliferate more rapidly after ~3 weeks in culture and were subsequently reseeded at $0.8–1.2 \times 10^5$ cells/25-cm^2 flask. Cultures in 20% O_2 began to populate with spontaneously immortalised, faster growing cells after 30–40 days and were subsequently reseeded at $0.8–1.2 \times 10^5$ cells/25-cm^2 flask.

The fold-population increase (PI) was calculated each time cells were counted (*# of cells counted / # of cells seeded = PI_1, PI_2, etc.*) and was used to calculate the cumulative population

increase (CumPI): $CumPI_1 = PI_1$, $CumPI_2 = PI_1 * PI_2$, $CumPI_3 = PI_1 * PI_2 * PI_3$, *etc.* The cumulative population increase was then used to calculate the cumulative population doubling (CumPD): $CumPD_1 = log2\ (CumPI_1)$, $CumPD_2 = log2\ (CumPI_2)$, *etc.*

2.8. Crystal violet staining assay for cell survival

The crystal violet staining assay [38] was used to determine relative cell survival following BaP or BPDE treatment, compared with control (untreated) cells. Cells were seeded on 96-well plates at 2.5–5.0 × 10^3/well and treated the following day with BaP (24 or 48 hr) or BPDE (2 hr) diluted in growth medium to a highest final concentration of 1 µM (0.1% DMSO final). BPDE treatment media was replaced after 2 hr with normal growth media. Treatment was performed in 5 replicate wells per condition at 37°C/5% CO_2/3% O_2. At 24 or 48 hr following initiation of treatment, cells were rinsed with PBS and adherent cells were fixed and stained for 15 min with 0.1% (*w/v*) crystal violet (Sigma #C3886) in 10% ethanol. Cells were gently washed with PBS to remove excess crystal violet and allowed to dry. For quantification, the dye was solubilised in 50% ethanol (100 µL per well) and absorbance at 595 nm was determined using a plate reader. Data are presented as the amount of absorbance in wells of treated cells relative to that of DMSO-treated cells and are representative of at least three independent experiments. The linearity of this method was confirmed for subconfluent HUF cultures (data not shown).

2.9. Carcinogen treatment of HUFs for DNA adduct analysis

The day prior to treatment, primary HUFs (Xpa-WT and Xpa-Null) were seeded so as to be sub-confluent at the time of harvest. For BaP treatment, 1.5 × 10^6 or 1.0 × 10^6 cells were seeded into 75-cm^2 flasks for treatments of 24 or 48 hr, respectively. For BPDE treatment (up to 2 hr), cells were seeded at 2.0–2.5 × 10^6 cells into 75-cm^2 flasks. Duplicate flasks were treated for each condition. BaP and BPDE were diluted in growth medium to a highest final concentration of 1 µM (0.1% DMSO final). Cells were incubated with BaP at 37°C/5% CO_2, in either 20% or 3% O_2, or with BPDE at 37°C/5% CO_2/3% O_2. Cells grown in medium containing 0.1% DMSO served as control. In the BPDE-DNA adduct removal experiment, treatment medium was removed after 2 hr and replaced with fresh growth medium. Cells were harvested following the indicated incubation time (BaP: 24 or 48 hr; BPDE: 0.5, 2 or 6 hr) and stored as pellets at –20°C until analysis. DNA adduct formation was assessed as described above.

2.10. Hupki mouse embryo fibroblast immortalisation assay (HIMA)

Immortalisation of primary Hupki mouse embryo fibroblasts treated with BPDE was performed twice (HIMA 1 and 2), according to previously published protocols [15, 39]. Frozen

Xpa-WT and Xpa-Null primary HUFs (passage 0) were thawed and seeded into 175-cm^2 flasks at 37°C/5% CO_2/3% O_2 for expansion. After 3 days, cells were trypsinised, counted and seeded (passage 1) at 2.0×10^5 cells/well into 6-well Corning CellBind® plates. Cells were treated the following day with 0.5 µM BPDE (for each *Xpa* genotype, HIMA 1: 48 cultures; HIMA 2: 54 cultures) or 0.1% DMSO (for each *Xpa* genotype, HIMA 1: 24 cultures; HIMA 2: 30 cultures) for 2 hr.

Following treatment, as the cells approached confluence, the HUFs were subcultured on 6-well Corning CellBind® plates at a dilution of 1:2–1:4. After a further 4 days, all cultures were transferred to 20% O_2 to select for senescence bypass. Cultures were passaged once or twice more at 1:2–1:4 before the cultures slowed significantly in their rate of proliferation, and began to show signs of senescence (large, flattened morphology). During senescent crisis, cultures were not passaged again until regions of dividing cells or clones had emerged, and were not diluted more than 1:2 until cells were able to repopulate a culture dish in less than 5 days after splitting. Cultures that did not contain dividing cells were passaged 1:1 every 2 weeks until clones developed. When immortal cells emerged from the senescent cultures and expanded into clones, serial passaging was resumed at dilutions of at least 1:2–1:4 for several passages, followed by further passaging at dilutions up to 1:20. Once a culture achieved a doubling rate of ≤ 48 hr and appeared homogeneous, it was progressively expanded from a 6-well plate to larger flasks (25-, 75-cm^2), frozen stocks were prepared and a portion of cells was pelleted for DNA extraction (≥ passage 12; 8–16 weeks).

2.11. TP53 mutation analysis

DNA was isolated from cell pellets using the Gentra Puregene Cell Kit B (Qiagen, #158745), according to the manufacturer's instructions. Human *TP53* sequences (exon 4 to exon 9, including introns) were amplified from each sample using the human *TP53*-specific primers and cycling conditions described in **Table S2**. Amplification products were assessed by electrophoresis on 2% agarose gels (containing 0.5 µg/mL ethidium bromide) in TBE buffer. Band size and intensity were monitored by loading 4 µL of Gel Pilot 100 bp Plus marker (Qiagen, #239045) onto each gel. To remove primers and deoxynucleoside triphosphates prior to sequencing, PCR reactions (12 µL) were digested with 2 U exonuclease I (New England Biolabs, UK, #M0293S) and 10 U shrimp alkaline phosphatase (USB Products, USA, #70092Y) for 20 min at 37°C followed by an inactivation step at 80°C for 15 min.

Samples were submitted to Beckman Coulter Genomics (Takeley, UK) for Sanger dideoxy fluorescent sequencing using the sequencing primers indicated in **Table S2**. Chromas software was used to export the FASTA sequence from the chromatograms which were also visually inspected. FASTA sequences were analysed by alignment against a human *TP53* reference sequence,

NC_000017.9 from Genbank, using the Basic Local Alignment Search Tool (BLAST) from the National Center for Biotechnology Information (NCBI) (http://blast.ncbi.nlm.nih.gov/Blast.cgi). Variations (*e.g.* single base substitutions, deletions) were assessed using the mutation validation tool available at the IARC TP53 mutation database (http://www-p53.iarc.fr/MutationValidationCriteria.asp), and could be classified as either homo-/hemi-zygous or heterozygous. Mutations were confirmed by sequencing DNA from an independent sample of cells from the same clone.

2.12. Statistical analysis

All statistical analyses were carried out using SAS v. 9.3 for Windows XP (SAS Institute, Cary, NC). The effects of Xpa status and chemical treatment (*i.e.* BaP or BPDE) on adduct formation were examined using ordinary least-squares 2-factor Analysis of Variance (ANOVA) followed by Bonferroni's post-hoc contrasts. Homogeneity of variance across the treatment groups was examined using the Bartlett test. Alternatively, pair-wise comparisons employed the Student's t test. The effects of Xpa status and chemical treatment (*i.e.* BPDE) on the frequency of *TP53* mutant clones or *TP53* mutation frequency were analysed using 2x2x2 contingency table analysis. The Chi-square test was used to test the null hypothesis that row (*i.e.* chemical treatment or Xpa status) and column (*i.e. TP53* mutant) variables are not significantly associated. Odds Ratio values were employed to assess the relative risk of a given outcome (*e.g. TP53* mutant) for paired levels of the chemical treatment or *Xpa* genotype (*e.g.* Xpa-Null versus Xpa-WT or BPDE-treated versus solvent control). The *exact* statement in Proc Freq provided exact tests and confidence limits for the Pearson Chi-square and Odds Ratio values. Since a small proportion of *TP53* mutant clones contained more than one mutation, the *TP53* mutation response was treated as an ordinally-scaled dependent variable (*i.e.* a multinomial response with outcome none, single or double). The effects of *Xpa* genotype and chemical treatment on mutation response were determined using ordinal logistic regression (*i.e.* cumulative logit model) in SAS Proc Catmod.

Pair-wise statistical comparisons of mutation patterns (*i.e.* type of mutations) employed a variation on the algorithm originally published by [40]; later modified by [41]. Briefly, statistical comparisons of mutation patterns for two conditions (*e.g.* Xpa-Null versus Xpa-WT for BPDE treated) were assessed using the Fisher's exact test with *P* values estimation determined using Monte Carlo simulation with 50,000 iterations.

3. Results

3.1. Creation of Xpa-deficient Hupki mice and embryos

Hupki mice deficient in NER were generated by crossing the Hupki strain with transgenic mice harbouring an *Xpa*-knockout allele. The *Hupki*$^{+/+}$;*Xpa*$^{-/-}$ offspring were healthy and did not show any obvious phenotypic differences from *Hupki*$^{+/+}$;*Xpa*$^{+/+}$ mice within the timeframe of these studies (up to 6 months). Likewise, Xpa-WT and Xpa-Null HUFs were morphologically similar.

3.2. BaP-induced DNA adduct formation in Xpa-WT and Xpa-Null Hupki mice

DNA adduct formation after treatment with BaP was initially assessed *in vivo* (**Fig. 1, Fig. S2 and Fig. S3**). One day following a single BaP treatment at 125 mg/kg bw, DNA adduct levels were significantly higher in three of six tissues examined (spleen, colon and kidney) from Xpa-Null mice compared with their WT littermates, ranging from 1.4- to 3.7-fold (**Fig. 1A**). Unexpectedly, all Xpa-Null mice died within 2–3 days of BaP (125 mg/kg bw) treatment (**Fig. 1B and Fig. S2**). In the Xpa-WT mice, BaP-DNA adduct levels following a single treatment persisted 5 days later in all tissues except the small intestine where there was a 2.5-fold decrease (**Fig. S2**). Further, DNA adduct levels greatly increased in Xpa-WT animals that received BaP daily for 5 days (14-, 12-, and 4-fold in liver, lung and small intestine, respectively) (**Fig. 1B**).

Due to the acute toxicity induced by BaP at 125 mg/kg bw in Xpa-Null mice, animals were treated with a 10-fold lower dose (*i.e.* 12.5 mg/kg bw) in a subsequent experiment (**Fig. 1C and D**). A single low dose of BaP (12.5 mg/kg bw) resulted in detectable DNA adducts in all tissues examined which exhibited a trend towards being higher in Xpa-Null mice compared to Xpa-WT mice (ranging from 1.8-fold [spleen] to 2.7-fold [small intestine]) (**Fig. 1C**) in line with the results obtained after a single administration of 125 mg/kg bw (compare to **Fig 1A**). Xpa-Null mice were able to tolerate 5 daily treatments with the lower dose of BaP. Interestingly, after 5 daily treatments, DNA adduct levels were about the same in Xpa-WT and Xpa-Null animals (**Fig. 1D**). Taken together, these experiments indicate that BaP-DNA adduct removal is dependent on Xpa/NER within 1 day of treatment, although NER fails to remove these adducts following 5 days of BaP exposure even in Xpa-WT mice. Further, the inability of Xpa-Null mice to repair BaP-DNA adducts can result in lethal toxicity if the DNA damage exceeds a certain threshold.

3.3. Growth of Xpa-WT and Xpa-Null HUFs at 20% and 3% oxygen

Due to the previously reported inhibition of culture-induced senescence of MEFs at 3% O_2, we sought to determine whether the growth of primary HUFs could also be enhanced and/or extended in 3% oxygen. Growth curves were generated over 6–9 weeks of culture in order to establish the

growth characteristics of both Xpa-WT and Xpa-Null HUFs in 20% and 3% oxygen (**Fig. 2A and B**).

In 20% O_2 the primary HUF cultures (Xpa-WT and Xpa-Null) rapidly proliferated for the first several days in culture (**Fig. 2A**). After 5 days the original populations had increased approximately 40-fold, and after 11 days the populations had increased about 200-fold. The proliferation of HUFs in 20% O_2 markedly decreased after 11–15 days, as cells began to senesce. The cultures resumed proliferation after 35–45 days as immortal cells emerged.

The HUF cultures grew rapidly in 3% O_2 for the first 11 days, at a slightly increased rate compared with cells grown in 20% O_2, doubling every 24–30 hr (**Fig. 2B**). After 5 days, the original populations had increased by 70-fold, and after 11 days they had increased by 2100-fold. After this point the cultures temporarily proliferated at a reduced rate (to varying degrees) and the cells appeared morphologically heterogeneous. By 25 days in culture in 3% O_2, cultures were again rapidly proliferating and were homogeneous in appearance.

Another set of HUF cultures was grown in 3% O_2 for 1 week and then transferred to 20% O_2, in order to determine whether cultures grown temporarily at 3% O_2 would still be capable of senescence and immortalisation at 20% O_2 (**Fig. S4**). Following transfer to 20% O_2, the cultures underwent 2 population doublings in the first 3 days of culture, but then slowed and began to senesce by the next passage. Similarly to cells grown continuously at 20% O_2, immortalised cells emerged in the cultures after 35–40 days.

3.4. Effect of oxygen on DNA adduct formation in HUFs treated with BaP

The growth curves generated in 20% and 3% O_2 indicated a clear growth advantage for primary HUFs grown in 3% O_2, at least prior to 2 weeks in culture. However, the impact of 3% *versus* 20% O_2 on the metabolic activation of carcinogens (*i.e.* BaP) has not been previously examined. Primary Xpa-WT HUFs grown in 20% and 3% O_2 (passage 1, $\leq$ 7 days in culture) were treated with 1 μM BaP for 24 or 48 hr to assess DNA adduct formation (**Fig. 2C**). Interestingly, DNA adduct levels were markedly higher in HUFs treated in 3% O_2 than in cells treated in 20% O_2. After 24 hr treatment, a 4-fold higher level of DNA adducts was detected in HUFs treated in 3% O_2 (513 ± 34 *versus* 129 ± 10 adducts per 10^8 nt) and after 48 hr treatment DNA adduct levels were 2-fold higher in 3% O_2 (839 ± 294 *versus* 391 ± 27 adducts per 10^8 nt) than in cells treated in 20% O_2. Therefore, growing HUFs temporarily in 3% O_2 not only provides a substantial increase in cells available for experiments, but may enhance the formation of DNA-reactive metabolites following treatment with environmental carcinogens. From these observations, all subsequent experiments were performed in 3% O_2.

3.5. Survival of Xpa-WT and Xpa-Null HUFs treated with BaP or its reactive intermediate BPDE

Previous studies using MEFs from *Xpa*-knockout mice (with WT *Trp53*) showed that Xpa-deficient cells are highly sensitive to DNA damage that is normally repaired by NER, including that induced by BaP [20, 42, 43]. Here, we have compared Xpa-Null HUFs with Xpa-WT HUFs for their sensitivity to BaP and its reactive intermediate BPDE. Xpa-Null HUFs were indeed more sensitive to treatment with both compounds, although the difference was more pronounced after 48 hr (**Fig. 3A and B**). Following treatment with 1 μM BaP, 63% of Xpa-Null cells had survived after 24 hr (91% for Xpa-WT), but by 48 hr BaP-treated Xpa-Null cells were 23% of control (60% for Xpa-WT) (**Fig. 3A**). Upon 1 μM BPDE treatment, 41% of Xpa-Null cells had survived after 24 hr (59% for Xpa-WT), but this had decreased to 6% at 48 hr (47% for Xpa-WT) (**Fig. 3B**). Interestingly, surviving Xpa-Null cells treated with ≥ 0.5 μM BaP did not resume proliferation, whereas those treated with ≤ 0.25 μM BaP resumed proliferation within 1–2 days of treatment (monitored visually with a microscope for up to two weeks; data not shown).

3.6. BaP- and BPDE-induced DNA adduct formation in Xpa-WT and Xpa-Null HUFs

Xpa-Null HUFs were shown to be highly sensitive to treatment with BaP and BPDE. Next, the level of DNA adducts induced by these compounds was assessed in Xpa-Null and Xpa-WT HUFs (**Fig. 3C and D**). Cells were treated with 0.05–1.0 μM of BaP for 24 hr or 0.125–1.0 μM BPDE for 2 hr. A concentration-dependent increase in DNA adduct formation was found after treatment with both compounds.

Interestingly, the Xpa-Null HUFs, despite being deficient in NER, accumulated similar or slightly lower levels of BaP-induced DNA adducts to Xpa-WT HUFs, reaching up to 370 ± 111 adducts per 10^8 nt at 1 μM BaP *versus* 513 ± 34 adducts per 10^8 nt in Xpa-WT HUFs. On the other hand, DNA adduct formation following BPDE treatment was slightly higher in Xpa-Null HUFs than in Xpa-WT HUFs, although the difference was significant only at the highest concentration of BPDE (1 μM) where DNA adduct levels reached 566 ± 88 adducts per 10^8 nt in Xpa-Null HUFs *versus* 475 ± 40 adducts per 10^8 nt in Xpa-WT HUFs.

Additionally, we examined a time course of BPDE adduct formation and removal in Xpa-WT and Xpa-Null HUFs. Previous studies have shown that the half-life of BPDE in cells is ~12 minutes and peak adduct formation appears to vary from 20 min to 2 hr, perhaps depending on cell type and experimental design [44-46]. Here, HUFs were treated with 0.25 μM BPDE for up to 2 hr, and one set of cultures was further incubated in normal medium for 4 hr after BPDE was removed. Cells were harvested to assess DNA adduct levels at 30 min, 2 hr and 6 hr (**Fig. S5**). Longer incubation times were not included to avoid effects caused by proliferation. After 30 min incubation with

BPDE, Xpa-Null and Xpa-WT HUFs accumulated the same level of DNA adducts (138 ± 1 adducts per 10^8 nt in both Xpa-Null and Xpa-WT HUFs). This initial DNA adduct level progressively declined in Xpa-WT HUFs, by 18% at 2 hr (114 ± 7 adducts per 10^8 nt) and by 30% at 6 hr (96 ± 12 adducts per 10^8 nt). In Xpa-Null HUFs, however, DNA adduct levels peaked at 2 hr (161 ± 19 adducts per 10^8 nucleotides), and were similar at 6 hr to the levels detected at 0.5 hr (132 ± 3 adducts per 10^8 nt). These results demonstrate that Xpa-WT HUFs are able to repair BPDE-DNA adducts over time, while the repair capacity of the Xpa-Null HUFs is impaired.

3.7. TP53 mutations induced by BPDE in Xpa-WT and Xpa-Null HUFs

3.7.1. Mutation frequency

Primary Xpa-WT and Xpa-Null HUF cultures (102 per genotype) were exposed for 2 hr to 0.5 μM BPDE and then serially passaged for 8–16 weeks (≥ 12 passages) in 20% O_2, resulting in one immortalised cell line per culture. Untreated cells of each *Xpa* genotype (54 cultures) were immortalised in parallel. Mutations in the human *TP53* sequence of immortalised HUF lines were identified by PCR amplification of exons 4–9 (along with adjacent introns) and direct dideoxy sequencing (**Tables 1 and 2**). From untreated HUF cultures, only two spontaneously immortalised lines of each *Xpa* genotype were found to contain mutated *TP53* (3.7%). Treatment with BPDE markedly increased the frequency of *TP53* mutations over that observed in untreated cultures. Of the 102 immortalised cell lines derived from BPDE-exposed Xpa-WT HUFs, 16 clones harboured a total of 20 mutations (four clones carried two mutations each), while 23 immortalised cell lines derived from BPDE-exposed Xpa-Null HUFs harboured a total of 29 mutations (six clones contained two mutations each). Statistical data analyses initially examined the effect of BPDE treatment on the frequency of *TP53* mutant clones, and confirmed a statistically significant effect for both Xpa-WT cells (*i.e.* Chi-squared = 5.0, $P < 0.04$) and Xpa-Null cells (*i.e.* Chi-squared = 9.3, $P < 0.003$). Similarly, the analyses showed a significant effect of BPDE treatment on *TP53* mutation frequency for Xpa-WT cells (*i.e.* Chi-squared = 4.1, $P < 0.05$) as well as Xpa-Null cells (*i.e.* Chi-squared = 7.1, $P < 0.008$). Furthermore, these data suggest a trend for an increased frequency of *TP53* mutagenesis in BPDE-exposed Xpa-Null HUFs (22.5%) compared with Xpa-WT HUFs (15.7%) that was confirmed by statistical analyses. More specifically, Odds Ratio values confirmed that Xpa-Null cells are more susceptible to the effects of BPDE treatment (*i.e.* OR = 7.6, 95% confidence interval = 1.7 to 33.5) as compared with Xpa-WT cells (*i.e.* OR = 4.8, 95% confidence interval = 1.1 to 21.9). However, the increase in the relative risk of *TP53* mutation between Xpa-Null and Xpa-WT HUFs is not statistically significant due to the relatively small number of mutants obtained and the consequently low statistical power. Indeed, separate statistical analysis that examined the impact of Xpa status on *TP53* mutation frequency for BPDE treated cells

only failed to detect a significant effect (*i.e.* Chi-squared = 1.9, *P* = 0.19, OR = 1.6 with 95% confidence interval = 0.83 to 3.0).

3.7.2. Mutation pattern

Most mutations induced by BPDE occurred at G:C base pairs (90% Xpa-WT; 83% Xpa-Null), predominantly consisting of single base substitutions (**Table 2 and Fig. 5**). The most frequent mutation type was a G:C>T:A transversion (40% Xpa-WT; 31% Xpa-Null), the signature mutation of BaP/BPDE, followed by G:C>C:G transversions (25% Xpa-WT; 21% Xpa-Null), and G:C>A:T transitions (20% Xpa-WT; 17% Xpa-Null). Single or tandem deletions of guanines, leading to a frameshift, were also observed but were more frequent in Xpa-Null clones (5% Xpa-WT; 14% Xpa-Null). Approximately half of the mutations at G:C base pairs occurred at CpG sites (56% Xpa-WT; 46% Xpa-Null). Out of 33 CpG sites between exons 4–9 in *TP53*, 11 were mutated by BPDE, most commonly resulting in G:C>C:G or G:C>T:A transversions. Of the four mutations found in untreated control cultures, one was a G:C>C:G transversion and three were A:T>C:G transversions. The A:T>C:G mutation type did not occur in BPDE-treated Xpa-WT HUFs but was found in three BPDE-treated Xpa-Null clones (XN-BP-278, -299, -300).

3.7.3. Strand bias

It has been shown previously that DNA damage induced by BPDE is repaired more rapidly if it occurs on the transcribed strand of *TP53* compared with the non-transcribed strand [47, 48]. This is thought to explain the strand bias of G to T mutations in *TP53* found in lung tumours of tobacco smokers, where mutations are preferentially found on the non-transcribed strand [49]. In contrast, in TC-NER-deficient cells mutations are biased in favour of the transcribed strand [50, 51]. Indeed, here we found an increased number of BPDE-induced mutations on the transcribed strand in Xpa-Null HUFs (38%) relative to Xpa-WT HUFs (10%) (**Table 1 and Fig. 4**). Statistical analysis to examine the influence of Xpa status on the transcribed and non-transcribed strand BPDE-induced *TP53* mutation frequencies, respectively, showed a statistically significant effect for the former, but not the latter. More specifically, Xpa status had a significant effect on the frequency of BPDE-induced mutations on the transcribed strand (*i.e.* Chi-squared = 6.5, *P* < 0.02). Moreover, the Odds Ratio confirmed a 6-fold increase in the average likelihood of BPDE-induced transcribed strand mutations for Xpa-Null cells compared to Xpa-WT cells (*i.e.* OR = 6.0, 95% confidence interval = 1.3 to 27.8). No such effect of Xpa status was observed for BPDE-induced *TP53* mutations on the non-transcribed strand (*i.e.* Chi-squared = 0.05, *P* = 0.86). All mutation types detected on the non-transcribed strand of Xpa-Null clones were also found on the transcribed strand, with the exception of A:T>T:A.

3.7.4. Effect of mutations on p53 protein function

The majority of BPDE-induced *TP53* mutations were missense (37/49). Additionally, three nonsense (R65X, W91X, E171X), three silent (P34P, V157V, L188L), one splice (acceptor site, intron 6) and five frameshift (codons 158, 189, 267, 330) mutations were induced, most of which occurred in Xpa-Null clones. All of the silent mutations occurred in clones that harboured a second mutation. Most of the missense mutations found in the immortalised HUF clones could be classified as 'non-functional' (NF), or defective in transactivation activity, as determined by a comprehensive yeast functional study [52]. This indicates, as shown previously, that loss of transactivation activity is an important aspect of senescence bypass by p53 inactivation [53]. However, eight missense mutations were classified as 'partially functional' (PF) or functional (F), whereby these p53 mutants retained some or all of their transactivation activity. Notably, all but one (R196G) of the PF/F mutants occurred in clones that also contained a second mutation, suggesting that partial loss of p53 transactivation function is not sufficient for senescence bypass.

3.7.5. Influence of sequence context

We also examined how sequence context and the presence of methylated CpG sites influenced the pattern of G:C base pair mutations induced by BPDE. In **Table S3** mutations of each type were sorted by the bases 5' and 3' to the mutated base. For G:C>A:T transitions, mutations occurred at CpG sites (2/9), at GG pairs (7/9; two of which were also CpG sites), or at G bases with a 5' or 3' T (4/9; two of which were also GG pairs). For G:C>C:G transversions, mutations occurred at CpG sites (7/11) or at GG pairs (7/11; three of which were also CpG sites). For G:C>T:A transversions, most mutations occurred at CpG sites (9/17), and the remaining mutations arose at GG pairs (6/17; one also being a CpG site) or in a 5'T-G-T3' context (3/17). Similarly, deletions at G:C base pairs occurred either at CpG sites (3/5) or at GG pairs. In the case of mutations occurring at GG pairs, the second G was 5' or 3' to the mutated base.

3.7.6 Codon distribution and comparison to human cancer mutation spectra

A total of 46 unique BPDE-induced mutations were detected in the sequenced exons (4–9), occurring in 38 codons overall. Three codons (158, 196, 273) were mutated in both Xpa-WT and Xpa-Null clones, but unique mutations were induced in each case. Mutations were found in codons for two key residues that make direct contact with the DNA (R248, R273), three that support the structure of the DNA binding surface (G245, R249, R282) and one that is important for coordinating Zn(2+) binding (C242).

The mutations identified in BPDE-exposed HUF clones were compared with *TP53* mutations found in human cancer across all tumour types, as well as specifically in lung cancer from smokers and non-smokers, using the IARC TP53 mutation database, version R17 (**Fig. 5**). All but five of the 46 *TP53* mutations found in BPDE-exposed HUFs have been detected in at least one human tumour (**Table S4**). Mutations that were infrequently or not found in human tumours included silent mutations, frameshifts, and mutations that resulted in a partially functional mutant p53 protein. Of the six hotspots most frequently mutated across all cancer types (R175, G245, R248, R249, R273, and R282), mutations were induced by BPDE at each, with the exception of R175. Further, BPDE also targeted two lung cancer-specific hotspots, codons V157 and R158. All of these hotspots, with the exception of codon 249, contain CpG sites.

At codon 157 (GTC), BPDE induced one G:C>T:A mutation at the 1st position and one G:C>A:T mutation at the 3rd position. At codon 158 (CGC), BPDE induced a G:C base pair deletion at the 1st position and two G:C>T:A mutations at the 2nd position. Codon 157 and 158 are more frequently targeted in smokers' lung cancer compared with cancer overall, with G:C>T:A transversions predominating (codon 157: 24/30; codon 158: 32/44). In cancer overall, G:C>T:A transversions are also the most common mutation type at codon 157 (210/313), but are less frequent at codon 158 (102/326), where G:C>A:T transitions at the second position are more common (113/326). No mutations at codons 157 or 158 have ever been detected in spontaneously immortalised HUFs (**Table S5**).

The most frequently mutated *TP53* codons in cancer overall and in smokers' lung cancer are 248 and 273 (**Fig. 5**). Likewise, these two codons were hotspots for BPDE-induced mutations in the current HIMA. In cancer overall and nonsmokers' lung cancer, the most frequent mutation type at codon 248 (CGG) is G:C>A:T (~90%), and indeed two of the mutations induced by BPDE were G:C>A:T transitions at the 2nd position. Additionally, one G:C>T:A mutation at the 2nd position was detected in the BPDE-treated HUFs. G:C>T:A transversions at the 2nd position in codon 248 are much more frequent in smokers' lung cancer (23/56) compared with all cancer (121/1880). Notably, mutation at codon 248 has not been detected in untreated, spontaneously immortalised HUFs (**Table S5**). With regards to codon 273 (CGT), BPDE-induced mutations included one G:C>T:A transversion at the first position, one G:C>C:G transversion at each of the 1st and 2nd positions, and two G:C>T:A mutations at the 2nd position. The most common mutation type found in human cancer at codon 273 is G:C>A:T (~90%); G:C>T:A transversions at the 2nd position are much more frequent in smokers' lung cancer (30/62). G:C>C:G mutations at codon 273 occur in 1-2% of cancer overall and 3-5% of smoker's lung cancer.

3.7.7 Comparison to mutations induced in previous HIMAs

BPDE-induced *TP53* mutations were compared further with mutations detected in previous HIMAs (**Table S5**), including HUFs treated with BaP, 3-NBA, AAI, UV and MNNG and untreated controls. Seven codons mutated by BPDE were also mutated in cells treated with BaP (135, 157, 158, 224, 248, 273, 282), and six identical mutations were induced by both compounds. Codons 157 and 224 were not mutated in HIMAs using other compounds. One mutation at codon 158 was induced by AAI, one mutation at codon 248 was induced by UV, and codon 273 was targeted once each by 3-NBA and AAI.

4. Discussion

We have generated an NER-deficient Hupki model by crossing the Hupki mouse with an *Xpa*-deficient mouse. We hypothesised that *Xpa*-deficiency would increase the sensitivity of the Hupki model to DNA damage normally repaired by NER and thereby increase the frequency of carcinogen-induced *TP53* mutations in immortalised HUFs. Xpa-WT and Xpa-Null mice and HUFs were treated with the ubiquitous environmental carcinogen BaP, or its reactive metabolite BPDE, which form DNA adducts (BPDE-N^2-dG) that have been shown to be repaired by the NER pathway. We found that Xpa-Null Hupki mice and HUFs were more sensitive than their Xpa-WT counterparts to the DNA damage induced by BaP or BPDE, exhibiting pronounced mortality at the highest doses tested. Further, we observed a bias for BPDE-induced mutations on the transcribed strand of *TP53* in immortal clones derived from Xpa-Null HUFs, although *TP53* mutation frequency overall was not significantly increased in Xpa-Null HUFs compared to Xpa-WT HUFs.

Although BaP- and BPDE-induced DNA adduct levels were generally similar between Xpa-WT and Xpa-Null HUFs, Xpa-Null cells were less able to survive the DNA damage. This suggests that the sensitivity of Xpa-Null cells was not due to retention of more DNA adducts. The sensitivity of Xpa-Null HUFs to BaP and BPDE is more likely caused by the blockage of RNAPII by BPDE-N^2-dG adducts in actively transcribed genes. The persistence of DNA lesions on the transcribed strand of active genes in TC-NER-deficient cells is a strong trigger for apoptosis induction [54]. It has been observed that Xpa-Null cells, deficient in both GG- and TC-NER, undergo apoptosis after DNA damage induced by carcinogens such as UV or BaP, whereas Xpc-Null cells, deficient only in GG-NER, do not, although this may be cell-type specific [55]. TC-NER-deficient cells are unable to repair RNAPII-blocking lesions; subsequent induction of apoptosis appears to occur during replication, possibly due to collision of DNA replication forks with stalled transcription complexes during S phase [56].

Xpa-Null Hupki mice were also highly sensitive to treatment with BaP; while treatment was well tolerated by Xpa-WT Hupki mice, Xpa-Null mice died within 2–3 days of receiving the highest dose tested (*i.e.* 125 mg/kg bw BaP). This sensitivity to genotoxins has been shown previously for Xpa-Null mice with WT *Trp53* after exposure to UV, 7,12-dimethylbenz[*a*]anthracene (DMBA), BaP and 2-amino-1-methyl-6-phenylimidazo[4,5-b]pyridine (PhIP) [18, 57]. As discussed above for HUFs, the sensitivity of Xpa-Null mice to these carcinogens is likely due to TC-NER deficiency and blockage of RNAPII by unrepaired DNA adducts. Xpc-Null mice, deficient only in GG-NER, do not share the same sensitivity [58]. One day following a single treatment with BaP, several tissues analysed from Xpa-Null Hupki mice had a higher level of BPDE-N^2-dG adducts compared with Xpa-WT mice. When the animals were treated with 5 daily doses of BaP (12.5 mg/kg bw), however, similar DNA adduct levels were detected in

Xpa-WT and Xpa-Null mice. This suggests that GG-NER is activated initially following BaP treatment in Xpa-WT mice, but is unable to deal with continuing damage. Interestingly, when BaP was previously tested in Xpa-Null and Xpa-WT mice with WT *Tp53* (3 doses of 13 mg/kg bw per week for 13 weeks), 9 weeks of treatment were required before DNA adduct levels in Xpa-Null mice surpassed those of Xpa-WT mice [22]; in that experiment DNA adduct formation was not assessed following a single treatment. Our results and those of others [22, 59] suggest that GG-NER kinetics of BPDE-N^2-dG adducts in NER-proficient mice is dose- and time-dependent. It is apparent that further investigations are required to explain these observations.

In addition to increased sensitivity to BPDE-N^2-dG adducts, Xpa-Null HUFs also exhibited enhanced BPDE-induced mutagenesis on the transcribed strand of *TP53* compared with Xpa-WT HUFs following BPDE treatment. These data further suggest that Xpa-Null HUFs are unable to repair BPDE-N^2-dG adducts on the transcribed strand; adducts that do not induce apoptosis may be converted to mutations. While the number of immortal Xpa-WT and Xpa-Null clones harbouring *TP53* mutations on the non-transcribed strand was nearly the same, 5.5-fold more Xpa-Null clones contained mutations on the transcribed strand compared to Xpa-WT clones. Further, the number of additional mutations on the transcribed strand induced by BPDE in Xpa-Null HUFs was equal to the overall increase in *TP53* mutations in Xpa-Null HUFs compared to Xpa-WT cells (see Table 1). This, and the accompanying statistical analyses, suggests that the increase in BPDE-induced *TP53*-mutagenesis in Xpa-Null HUFs compared to Xpa-WT cells can be primarily be accounted for by the inability of Xpa-Null HUFs to repair damage on the transcribed strand.

It is unclear why Xpa-deficiency did not also increase *TP53* mutagenesis on the non-transcribed strand. It is known that repair of BPDE-DNA adducts is slower on the non-transcribed strand compared to the transcribed strand in the *TP53* gene of normal human fibroblasts, creating a bias of mutations on the non-transcribed strand in NER-proficient cells [47]. Despite the relative inefficiency of GG-NER compared to TC-NER, BPDE-DNA adduct removal from the bulk of the genome has been shown, to varying extents, in multiple studies. The amount of removal within 8 hr of BPDE exposure ranged between 5–60% in normal human fibroblasts [60], to 50% in V79-XEM2 cells [45], to 75% removal in A549 lung carcinoma cells [44]. In the current study, we found that Xpa-WT HUFs removed 30% of BPDE-N^2-dG adducts within 6 hr of treatment. It is not known what percentage of BPDE-N^2-dG adducts may have persisted in the HUF genomes beyond this time-point.

Few studies have compared BaP/BPDE-induced mutagenesis in NER-proficient and NER-deficient cells. Xpa-Null mouse embryonic stem cells treated with BaP exhibited a higher rate of *Hprt* mutations than their WT counterparts, although the Xpa-Null cells also had a higher rate of spontaneous mutagenesis [43]. Further, more *Hprt* mutations were induced by BPDE in an NER-

defective Chinese hamster ovary cell line (UV5) relative to a WT line (AA8) [45]. On the other hand, *in vivo*, similar mutation frequencies at a *lacZ* reporter gene were detected in the liver and lung of BaP-treated Xpa-Null and Xpa-WT mice; *lacZ* mutation frequencies did increase in the spleens of Xpa-Null mice, but only after 13 weeks of BaP treatment [22]. Thus, the impact of NER-deficiency on mutagenesis resulting from BPDE-N^2-dG adducts may be cell-type specific or dependent on the target gene of interest and whether or not the gene is subject to TC-NER (*e.g. lacZ* is not transcribed by mammalian cells).

In agreement with previous studies, the majority of BPDE-induced *TP53* mutations occurred at G:C base pairs in both Xpa-WT and Xpa-Null HUFs, with G:C>T:A transversions being the predominant mutation type [14, 61, 62]. A high percentage (46–56%) of the mutations at G:C base pairs occurred at CpG sites; G:C>C:G and G:C>T:A transversions were more common at these sites than G:C>A:T transitions. Further, we found that BPDE induced mutations at several sites that are hotspots for mutation in cancer overall (codons 245, 248, 249, 273, 282), or smokers' lung cancer specifically (codons 157 and 158, in addition to those listed for cancer overall). Codons 157, 158 and 273 were also mutated in prior HIMAs with BaP-treated HUFs [14].

The pattern and spectrum of *TP53* mutagenesis can be influenced by a number of factors. In previous studies DNA adduct formation by BPDE was enhanced at methylated CpG sites in *TP53* hotspot codons 157, 158, 245, 248, and 273 on the non-transcribed strand [63, 64]; the precise mechanism underlying this phenomenon is not yet understood. It has been proposed that the methyl group of 5-methylcytosine allows increased intercalation of BPDE at methylated CpG sites and that this increase in BPDE intercalative binding subsequently results in increased covalent interaction [65, 66]. Others have suggested that the methylation of cytosine enhances the nucleophilicity of the exocyclic amino group of the base paired guanine (electronic effect) [67]. All of the CpG sites in Hupki *TP53* are methylated [68]. Interestingly, codon 179 (CAT), which is a mutation hotspot in smokers' lung cancer but does not contain a CpG site or a G on the non-transcribed strand, was not mutated by BPDE in our study and was not targeted by BPDE in normal human bronchial epithelial (NHBE) cells [69]. On the other hand, codon 267 (CGG), which is infrequently mutated in lung cancer but does harbour a CpG site, was mutated by BPDE in two HUF clones and exhibited pronounced BPDE-DNA adduct formation in NHBE cells [69]. Our data provide additional support for the idea that certain *TP53* mutation hotspots (*i.e.* codons 157, 158, 248, 273) act as selective BPDE binding sites.

Additional factors such as sequence context, efficiency of lesion repair (as discussed above), and fidelity of translesion synthesis polymerases also play important roles in *TP53* mutagenesis. We found that a common context for BPDE-induced single base substitutions or deletions at G:C base pairs was GG dinucleotide sequences; mutation hotspots for BPDE-N^2-dG adducts have previously

been found in such sequences [70, 71]. Sequence context likely influences adduct conformation which may result in different sequence-dependent removal rates of the lesion and also control mutagenic specificity.

Furthermore, the *TP53* mutations ultimately observed in human cancers are strongly influenced by functional selection for mutants that have a deleterious impact on the normal function of p53 or that acquire gain-of-function properties [6]. For example, many mutation hotspots occur at codons for amino acids that are essential for DNA contact (248, 273) or structure of the DNA binding domain (175, 245, 249, 282); mutations at these sites create a mutant protein that lacks the ability to transactivate the normal suite of p53 target genes. With the exception of codon 175, all of these hotspots were mutated by BPDE in our study. Further, most of the missense *TP53* mutations detected in our study were classified as non-functional and, with one exception, the mutations that retained some functionality occurred only in clones that also harboured a non-functional mutation. Taken together, the pattern and spectrum of mutations generated in this study indicate that similar factors influence *TP53* mutagenesis in the HUF immortalisation assay and human cancer, further supporting the strength of this model for assessing the effects of carcinogens on this tumour suppressor gene.

We also showed that the replicative capacity of primary HUFs could be extended by culturing the cells at 3% O_2. After 11 days of culture, the population increase of HUFs grown at 3% O_2 was 10-fold higher than that of HUFs grown at 20% O_2. The enhanced growth permitted by temporary culture in 3% O_2 provides a substantial increase in cells available for further experiments. To select for *TP53*-mutated cells, HUFs must eventually be transferred to 20% O_2, where the ability of cells to bypass senescence serves as the selection pressure for mutants. Importantly, we found that untreated HUFs grown at 3% O_2 for one week were still able to senesce when transferred to 20% O_2, and immortal variants that bypassed senescence developed in a similar timeframe to cells maintained at 20% O_2. Parrinello *et al.* found that MEFs cultured at 3% O_2 for more than 15 population doublings ($\geq$ 30 days) lost their propensity to senesce at 20% O_2, which they speculated may be due to a mutagenic event or adaptive response [37]. It may therefore only be beneficial to culture HUFs for 1–2 weeks at 3% O_2.

In addition to a clear growth advantage, we found that HUFs accumulated a higher level (2–4 fold) of DNA adducts at 3% O_2 relative to 20% O_2 following treatment with BaP. We did not determine the mechanism for this in our study, but future work could examine the expression/activity of enzymes required for BaP activation (*i.e.* Cyp1a1 and Cyp1b1) at 3% O_2 and 20% O_2. Recent work by van Schooten *et al.*, using the human lung carcinoma cell line A549 treated with BaP, has shown that the level of DNA adducts and the gene expression of *CYP1A1* and *CYP1B1* was increased under hypoxic conditions (0.2% O_2), while gene expression of UDP-

glucuronosyltransferase detoxifying enzymes *UGT1A6* and *UGT2B7* decreased [72]. The authors concluded that the balance of metabolism of BaP shifts towards activation instead of detoxification under low oxygen conditions. These results corroborate our findings that altered oxygen levels can influence the metabolic activation of compounds such as BaP.

Although we were unable to detect a significant increase in BPDE-induced *TP53* mutations overall in Xpa-Null HUFs compared to Xpa-WT HUFs, perhaps a divergence in mutation frequency would be evident at the genome-wide level. Less than 25% of HUF clones were immortalised by *TP53* mutation, thus other genes are clearly involved in senescence bypass by HUFs and could also be targeted by BPDE [53]. Recently, exome sequencing of DNA from HUFs treated with various mutagens (*e.g.* BaP and AAI) was used to extract genome-wide mutational signatures of mutagen exposure [73]. This study demonstrates that a single mutagen-treated immortal HUF clone harbours hundreds of single base substitutions at the exome level, likely consisting of both immortalisation driver mutations and passenger mutations. Therefore, whole-genome sequence analysis of BPDE-treated Xpa-WT and Xpa-Null clones may allow differences in mutation frequency in the context of the genome to be detected that are not observed in an assay for a single gene. Furthermore, beyond simply increasing mutation frequencies, Xpa-Null HUFs may be useful in the future to enhance our understanding of the role of NER in shaping carcinogen-induced mutagenesis of both *TP53* and the genome.

Acknowledgements

Jill E. Kucab was funded by a PhD studentship (2008-2012) from the Institute of Cancer Research, London, U.K. Work at King's College London was supported by Cancer Research UK (grant C313AA14329) and the Wellcome Trust (grant WT101126/B/13/Z). Jill E. Kucab, David H. Phillips and Volker M. Arlt are members of the Wellcome Trust funded COMSIG (Causes of Mutational SIGnatures) consortium. We are grateful for statistical advice and assistance provided by Rémi Gagné and Andrew Williams, Health Canada, Ottawa.

References

[1] D.P. Lane, Cancer. p53, guardian of the genome, Nature, 358 (1992) 15-16.
[2] K.H. Vousden, X. Lu, Live or let die: the cell's response to p53, Nat Rev Cancer, 2 (2002) 594-604.
[3] T. Riley, E. Sontag, P. Chen, A. Levine, Transcriptional control of human p53-regulated genes, Nat Rev Mol Cell Biol, 9 (2008) 402-412.
[4] M. Hollstein, D. Sidransky, B. Vogelstein, C.C. Harris, p53 mutations in human cancers, Science, 253 (1991) 49-53.
[5] P. Hainaut, M. Hollstein, p53 and human cancer: the first ten thousand mutations, Adv Cancer Res, 77 (2000) 81-137.
[6] M. Olivier, M. Hollstein, P. Hainaut, TP53 mutations in human cancers: origins, consequences, and clinical use, Cold Spring Harbor perspectives in biology, 2 (2010) a001008.
[7] A. Petitjean, E. Mathe, S. Kato, C. Ishioka, S.V. Tavtigian, P. Hainaut, M. Olivier, Impact of mutant p53 functional properties on TP53 mutation patterns and tumor phenotype: lessons from recent developments in the IARC TP53 database, Hum Mutat, 28 (2007) 622-629.
[8] A.J. Schetter, C.C. Harris, Tumor suppressor p53 (TP53) at the crossroads of the exposome and the cancer genome, Proc Natl Acad Sci U S A, 109 (2012) 7955-7956.
[9] J.L. Luo, Q. Yang, W.M. Tong, M. Hergenhahn, Z.Q. Wang, M. Hollstein, Knock-in mice with a chimeric human/murine p53 gene develop normally and show wild-type p53 responses to DNA damaging agents: a new biomedical research tool, Oncogene, 20 (2001) 320-328.
[10] J.E. Kucab, D.H. Phillips, V.M. Arlt, Linking environmental carcinogen exposure to TP53 mutations in human tumours using the human TP53 knock-in (Hupki) mouse model, FEBS J, 277 (2010) 2567-2583.
[11] A. Besaratinia, G.P. Pfeifer, Applications of the human p53 knock-in (Hupki) mouse model for human carcinogen testing, FASEB journal : official publication of the Federation of American Societies for Experimental Biology, 24 (2010) 2612-2619.
[12] Z. Liu, M. Hergenhahn, H.H. Schmeiser, G.N. Wogan, A. Hong, M. Hollstein, Human tumor p53 mutations are selected for in mouse embryonic fibroblasts harboring a humanized p53 gene, Proc Natl Acad Sci U S A, 101 (2004) 2963-2968.
[13] Z. Liu, K.R. Muehlbauer, H.H. Schmeiser, M. Hergenhahn, D. Belharazem, M.C. Hollstein, p53 mutations in benzo(a)pyrene-exposed human p53 knock-in murine fibroblasts correlate with p53 mutations in human lung tumors, Cancer Res, 65 (2005) 2583-2587.
[14] M. Reinbold, J.L. Luo, T. Nedelko, B. Jerchow, M.E. Murphy, C. Whibley, Q. Wei, M. Hollstein, Common tumour p53 mutations in immortalized cells from Hupki mice heterozygous at codon 72, Oncogene, 27 (2008) 2788-2794.
[15] T. Nedelko, V.M. Arlt, D.H. Phillips, M. Hollstein, TP53 mutation signature supports involvement of aristolochic acid in the aetiology of endemic nephropathy-associated tumours, Int J Cancer, 124 (2009) 987-990.
[16] E.C. Friedberg, How nucleotide excision repair protects against cancer, Nat Rev Cancer, 1 (2001) 22-33.
[17] O.D. Scharer, Nucleotide excision repair in eukaryotes, Cold Spring Harbor perspectives in biology, 5 (2013) a012609.
[18] A. de Vries, C.T. van Oostrom, F.M. Hofhuis, P.M. Dortant, R.J. Berg, F.R. de Gruijl, P.W. Wester, C.F. van Kreijl, P.J. Capel, H. van Steeg, et al., Increased susceptibility to ultraviolet-B and carcinogens of mice lacking the DNA excision repair gene XPA, Nature, 377 (1995) 169-173.
[19] R.J. Berg, A. de Vries, H. van Steeg, F.R. de Gruijl, Relative susceptibilities of XPA knockout mice and their heterozygous and wild-type littermates to UVB-induced skin cancer, Cancer Res, 57 (1997) 581-584.
[20] H. van Steeg, A. de Vries, C. van Oostrom, J. van Benthem, R.B. Beems, C.F. van Kreijl, DNA repair-deficient Xpa and Xpa/p53+/- knock-out mice: nature of the models, Toxicol Pathol, 29 Suppl (2001) 109-116.

[21] J.C. Klein, R.B. Beems, P.E. Zwart, M. Hamzink, G. Zomer, H. van Steeg, C.F. van Kreijl, Intestinal toxicity and carcinogenic potential of the food mutagen 2-amino-1-methyl-6-phenylimidazo[4,5-b]pyridine (PhIP) in DNA repair deficient XPA–/– mice, Carcinogenesis, 22 (2001) 619-626.
[22] A. de Vries, M.E. Dolle, J.L. Broekhof, J.J. Muller, E.D. Kroese, C.F. van Kreijl, P.J. Capel, J. Vijg, H. van Steeg, Induction of DNA adducts and mutations in spleen, liver and lung of XPA-deficient/lacZ transgenic mice after oral treatment with benzo[a]pyrene: correlation with tumour development, Carcinogenesis, 18 (1997) 2327-2332.
[23] E.M. Hoogervorst, A. de Vries, R.B. Beems, C.T. van Oostrom, P.W. Wester, J.G. Vos, W. Bruins, M. Roodbergen, F.R. Cassee, J. Vijg, F.J. van Schooten, H. van Steeg, Combined oral benzo[a]pyrene and inhalatory ozone exposure have no effect on lung tumor development in DNA repair-deficient Xpa mice, Carcinogenesis, 24 (2003) 613-619.
[24] H. Rebel, L.O. Mosnier, R.J. Berg, A. Westerman-de Vries, H. van Steeg, H.J. van Kranen, F.R. de Gruijl, Early p53-positive foci as indicators of tumor risk in ultraviolet-exposed hairless mice: kinetics of induction, effects of DNA repair deficiency, and p53 heterozygosity, Cancer Res, 61 (2001) 977-983.
[25] B.N. Ames, J. McCann, E. Yamasaki, Methods for detecting carcinogens and mutagens with the Salmonella/mammalian-microsome mutagenicity test, Mutat Res, 31 (1975) 347-364.
[26] L.H. Thompson, E.P. Salazar, K.W. Brookman, C.A. Hoy, Hypersensitivity to cell killing and mutation induction by chemical carcinogens in an excision repair-deficient mutant of CHO cells, Mutat Res, 112 (1983) 329-344.
[27] K. Tanaka, S. Kamiuchi, Y. Ren, R. Yonemasu, M. Ichikawa, H. Murai, M. Yoshino, S. Takeuchi, M. Saijo, Y. Nakatsu, H. Miyauchi-Hashimoto, T. Horio, UV-induced skin carcinogenesis in xeroderma pigmentosum group A (XPA) gene-knockout mice with nucleotide excision repair-deficiency, Mutat Res, 477 (2001) 31-40.
[28] V.M. Arlt, M. Stiborova, C.J. Henderson, M. Thiemann, E. Frei, D. Aimova, R. Singh, G. Gamboa da Costa, O.J. Schmitz, P.B. Farmer, C.R. Wolf, D.H. Phillips, Metabolic activation of benzo[a]pyrene in vitro by hepatic cytochrome P450 contrasts with detoxification in vivo: experiments with hepatic cytochrome P450 reductase null mice, Carcinogenesis, 29 (2008) 656-665.
[29] M. Stiborova, M. Moserova, V. Cerna, R. Indra, M. Dracinsky, M. Sulc, C.J. Henderson, C.R. Wolf, H.H. Schmeiser, D.H. Phillips, E. Frei, V.M. Arlt, Cytochrome b5 and epoxide hydrolase contribute to benzo[a]pyrene-DNA adduct formation catalyzed by cytochrome P450 1A1 under low NADPH:P450 oxidoreductase conditions, Toxicology, 318 (2014) 1-12.
[30] H. Naegeli, N.E. Geacintov, Mechanisms of Repair of Polycyclic Aromatic Hydrocarbon-Induced DNA Damage, in: The Carcinogenic Effects of Polycyclic Aromatic Hydrocarbons, pp. 211-258.
[31] R.G. Harvey, P.P. Fu, Synthesis and reactions of diol epoxides and related metabolites of carcinogenic hydrocarbons., in: H.V. Gelboin, P.O.P. Ts'o (Eds.) *Polycyclic Hydrocarbons and Cancer*, Academic Press, New York, 1978, pp. pp. 133-165.
[32] V.M. Arlt, M.C. Poirier, S.E. Sykes, K. John, M. Moserova, M. Stiborova, C. Roland Wolf, C.J. Henderson, D.H. Phillips, Exposure to benzo[a]pyrene of Hepatic Cytochrome P450 Reductase Null (HRN) and P450 Reductase Conditional Null (RCN) mice: Detection of benzo[a]pyrene diol epoxide-DNA adducts by immunohistochemistry and (32)P-postlabelling, Toxicol Lett, 213 (2012) 160-166.
[33] D.H. Phillips, V.M. Arlt, (3)(2)P-postlabeling analysis of DNA adducts, Methods in molecular biology (Clifton, N.J.), 1105 (2014) 127-138.
[34] S.L. Hockley, V.M. Arlt, G. Jahnke, A. Hartwig, I. Giddings, D.H. Phillips, Identification through microarray gene expression analysis of cellular responses to benzo(a)pyrene and its diol-epoxide that are dependent or independent of p53, Carcinogenesis, 29 (2008) 202-210.
[35] M. Csete, Oxygen in the cultivation of stem cells, Ann N Y Acad Sci, 1049 (2005) 1-8.

[36] P.J. Hornsby, Mouse and human cells versus oxygen, Sci Aging Knowledge Environ, 2003 (2003) PE21.
[37] S. Parrinello, E. Samper, A. Krtolica, J. Goldstein, S. Melov, J. Campisi, Oxygen sensitivity severely limits the replicative lifespan of murine fibroblasts, Nat Cell Biol, 5 (2003) 741-747.
[38] T.P. Dooley, R.C. Gadwood, K. Kilgore, L.M. Thomasco, Development of an in vitro primary screen for skin depigmentation and antimelanoma agents, Skin Pharmacol, 7 (1994) 188-200.
[39] Z. Liu, D. Belharazem, K.R. Muehlbauer, T. Nedelko, Y. Knyazev, M. Hollstein, Mutagenesis of human p53 tumor suppressor gene sequences in embryonic fibroblasts of genetically-engineered mice, Genet Eng (N Y), 28 (2007) 45-54.
[40] W.T. Adams, T.R. Skopek, Statistical test for the comparison of samples from mutational spectra, Journal of molecular biology, 194 (1987) 391-396.
[41] N.F. Cariello, W.W. Piegorsch, W.T. Adams, T.R. Skopek, Computer program for the analysis of mutational spectra: application to p53 mutations, Carcinogenesis, 15 (1994) 2281-2285.
[42] S.L. Colton, X.S. Xu, Y.A. Wang, G. Wang, The involvement of ataxia-telangiectasia mutated protein activation in nucleotide excision repair-facilitated cell survival with cisplatin treatment, J Biol Chem, 281 (2006) 27117-27125.
[43] T. Ogi, Y. Shinkai, K. Tanaka, H. Ohmori, Polkappa protects mammalian cells against the lethal and mutagenic effects of benzo[a]pyrene, Proc Natl Acad Sci U S A, 99 (2002) 15548-15553.
[44] K. Dreij, A. Seidel, B. Jernstrom, Differential removal of DNA adducts derived from anti-diol epoxides of dibenzo[a,l]pyrene and benzo[a]pyrene in human cells, Chem Res Toxicol, 18 (2005) 655-664.
[45] A. Lagerqvist, D. Hakansson, G. Prochazka, C. Lundin, K. Dreij, D. Segerback, B. Jernstrom, M. Tornqvist, A. Seidel, K. Erixon, D. Jenssen, Both replication bypass fidelity and repair efficiency influence the yield of mutations per target dose in intact mammalian cells induced by benzo[a]pyrene-diol-epoxide and dibenzo[a,l]pyrene-diol-epoxide, DNA Repair (Amst), 7 (2008) 1202-1212.
[46] D.R. Lloyd, P.C. Hanawalt, p53-dependent global genomic repair of benzo[a]pyrene-7,8-diol-9,10-epoxide adducts in human cells, Cancer Res, 60 (2000) 517-521.
[47] M.F. Denissenko, A. Pao, G.P. Pfeifer, M. Tang, Slow repair of bulky DNA adducts along the nontranscribed strand of the human p53 gene may explain the strand bias of transversion mutations in cancers, Oncogene, 16 (1998) 1241-1247.
[48] J.M. Ford, L. Lommel, P.C. Hanawalt, Preferential repair of ultraviolet light-induced DNA damage in the transcribed strand of the human p53 gene, Mol Carcinog, 10 (1994) 105-109.
[49] G.P. Pfeifer, P. Hainaut, On the origin of G --> T transversions in lung cancer, Mutat Res, 526 (2003) 39-43.
[50] R.H. Chen, V.M. Maher, J.J. McCormick, Lack of a cell cycle-dependent strand bias for mutations induced in the HPRT gene by (+/-)-7 beta,8 alpha-dihydroxy-9 alpha,10 alpha-epoxy-7,8,9,10-tetrahydrobenzo(a)pyrene in excision repair-deficient human cells, Cancer Res, 51 (1991) 2587-2592.
[51] M. Schiltz, X.X. Cui, Y.P. Lu, H. Yagi, D.M. Jerina, M.Z. Zdzienicka, R.L. Chang, A.H. Conney, S.J. Wei, Characterization of the mutational profile of (+)-7R,8S-dihydroxy-9S, 10R-epoxy-7,8,9,10-tetrahydrobenzo[a]pyrene at the hypoxanthine (guanine) phosphoribosyltransferase gene in repair-deficient Chinese hamster V-H1 cells, Carcinogenesis, 20 (1999) 2279-2286.
[52] S. Kato, S.Y. Han, W. Liu, K. Otsuka, H. Shibata, R. Kanamaru, C. Ishioka, Understanding the function-structure and function-mutation relationships of p53 tumor suppressor protein by high-resolution missense mutation analysis, Proc Natl Acad Sci U S A, 100 (2003) 8424-8429.
[53] C. Whibley, A.F. Odell, T. Nedelko, G. Balaburski, M. Murphy, Z. Liu, L. Stevens, J.H. Walker, M. Routledge, M. Hollstein, Wild-type and Hupki (human p53 knock-in) murine embryonic fibroblasts: p53/ARF pathway disruption in spontaneous escape from senescence, J Biol Chem, 285 (2010) 11326-11335.
[54] M. Ljungman, F. Zhang, Blockage of RNA polymerase as a possible trigger for u.v. light-induced apoptosis, Oncogene, 13 (1996) 823-831.

[55] H. de Waard, E. Sonneveld, J. de Wit, R. Esveldt-van Lange, J.H. Hoeijmakers, H. Vrieling, G.T. van der Horst, Cell-type-specific consequences of nucleotide excision repair deficiencies: Embryonic stem cells versus fibroblasts, DNA Repair (Amst), 7 (2008) 1659-1669.
[56] M. Ljungman, D.P. Lane, Transcription - guarding the genome by sensing DNA damage, Nat Rev Cancer, 4 (2004) 727-737.
[57] K. Imaida, K. Ogawa, S. Takahashi, T. Ito, T. Yamaguchi, Y. Totsuka, K. Wakabayashi, K. Tanaka, N. Ito, T. Shirai, Delay of DNA-adduct repair and severe toxicity in xeroderma pigmentosum group A gene (XPA) deficient mice treated with 2-amino-1-methyl-6-phenyl-imidazo [4,5-b] pyridine (PhIP), Cancer Lett, 150 (2000) 63-69.
[58] R.J. Berg, H.J. Ruven, A.T. Sands, F.R. de Gruijl, L.H. Mullenders, Defective global genome repair in XPC mice is associated with skin cancer susceptibility but not with sensitivity to UVB induced erythema and edema, J Invest Dermatol, 110 (1998) 405-409.
[59] P.C. van Kesteren, P.E. Zwart, M.M. Schaap, T.E. Pronk, M.H. van Herwijnen, J.C. Kleinjans, B.G. Bokkers, R.W. Godschalk, M.J. Zeilmaker, H. van Steeg, M. Luijten, Benzo[a]pyrene-induced transcriptomic responses in primary hepatocytes and in vivo liver: Toxicokinetics is essential for in vivo-in vitro comparisons, Arch Toxicol, (2012) Epub 2012/2010/2012.
[60] S. Venkatachalam, M. Denissenko, A.A. Wani, DNA repair in human cells: quantitative assessment of bulky anti-BPDE-DNA adducts by non-competitive immunoassays, Carcinogenesis, 16 (1995) 2029-2036.
[61] B. Ruggeri, M. DiRado, S.Y. Zhang, B. Bauer, T. Goodrow, A.J. Klein-Szanto, Benzo[a]pyrene-induced murine skin tumors exhibit frequent and characteristic G to T mutations in the p53 gene, Proc Natl Acad Sci U S A, 90 (1993) 1013-1017.
[62] E. Eisenstadt, A.J. Warren, J. Porter, D. Atkins, J.H. Miller, Carcinogenic epoxides of benzo[a]pyrene and cyclopenta[cd]pyrene induce base substitutions via specific transversions, Proc Natl Acad Sci U S A, 79 (1982) 1945-1949.
[63] M.F. Denissenko, J.X. Chen, M.S. Tang, G.P. Pfeifer, Cytosine methylation determines hot spots of DNA damage in the human P53 gene, Proc Natl Acad Sci U S A, 94 (1997) 3893-3898.
[64] G.P. Pfeifer, p53 mutational spectra and the role of methylated CpG sequences, Mutat Res, 450 (2000) 155-166.
[65] N.E. Geacintov, M. Shahbaz, V. Ibanez, K. Moussaoui, R.G. Harvey, Base-sequence dependence of noncovalent complex formation and reactivity of benzo[a]pyrenediol epoxide with polynucleotides, Biochemistry, 27 (1988) 8380-8387.
[66] L.C. Sowers, B.R. Shaw, W.D. Sedwick, Base stacking and molecular polarizability: effect of a methyl group in the 5-position of pyrimidines, Biochemical and biophysical research communications, 148 (1987) 790-794.
[67] W.S. Johnson, Q.Y. He, M. Tomasz, Selective recognition of the m5CpG dinucleotide sequence in DNA by mitomycin C for alkylation and cross-linking, Bioorganic & medicinal chemistry, 3 (1995) 851-860.
[68] S.I. Kim, M. Hollstein, G.P. Pfeifer, A. Besaratinia, Unveiling the methylation status of CpG dinucleotides in the substituted segment of the human p53 knock-in (Hupki) mouse genome, Mol Carcinog, 49 (2010) 999-1006.
[69] M.F. Denissenko, A. Pao, M. Tang, G.P. Pfeifer, Preferential formation of benzo[a]pyrene adducts at lung cancer mutational hotspots in P53, Science, 274 (1996) 430-432.
[70] F.A. Rodriguez, Y. Cai, C. Lin, Y. Tang, A. Kolbanovskiy, S. Amin, D.J. Patel, S. Broyde, N.E. Geacintov, Exocyclic amino groups of flanking guanines govern sequence-dependent adduct conformations and local structural distortions for minor groove-aligned benzo[a]pyrenyl-guanine lesions in a GG mutation hotspot context, Nucleic acids research, 35 (2007) 1555-1568.
[71] H. Rodriguez, E.L. Loechler, Mutational specificity of the (+)-anti-diol epoxide of benzo[a]pyrene in a supF gene of an Escherichia coli plasmid: DNA sequence context influences hotspots, mutagenic specificity and the extent of SOS enhancement of mutagenesis, Carcinogenesis, 14 (1993) 373-383.

[72] F.J. van Schooten, M. Schults, K. Sanen, R. Godschalk, J. Theys, R. Chiu, Hypoxia affects the metabolic activation and detoxification of the environmental mutagen benzo(a)pyrene, in: Proceedings of the 103rd Annual Meeting of the American Association for Cancer Research, Cancer Reasearch, Chicago, IL, 2012, pp. Abstract 4118.
[73] M. Olivier, A. Weninger, M. Ardin, H. Huskova, X. Castells, M.P. Vallee, J. McKay, T. Nedelko, K.R. Muehlbauer, H. Marusawa, J. Alexander, L. Hazelwood, G. Byrnes, M. Hollstein, J. Zavadil, Modelling mutational landscapes of human cancers in vitro, Scientific reports, 4 (2014) 4482.
[74] D.M. DeMarini, S. Landi, D. Tian, N.M. Hanley, X. Li, F. Hu, B.C. Roop, M.J. Mass, P. Keohavong, W. Gao, M. Olivier, P. Hainaut, J.L. Mumford, Lung tumor KRAS and TP53 mutations in nonsmokers reflect exposure to PAH-rich coal combustion emissions, Cancer Res, 61 (2001) 6679-6681.
[75] F.H. Sarkar, Y. Li, V. Vallyathan, Molecular analysis of p53 and K-ras in lung carcinomas of coal miners, International journal of molecular medicine, 8 (2001) 453-459.

Table 1. Summary of *TP53* mutation frequency and patterns in immortalised clones of Xpa-WT and Xpa-Null HUFs treated with BPDE and from spontaneously immortalised controls.

BPDE	Xpa-WT	Xpa-Null
Total BPDE-treated HUF cultures (#)	102	102
TP53 -mutant immortalised clones (#)	16	23
Total *TP53* mutations detected (#)	20	29
Frequency of *TP53* -mutant clones	15.7% (16/102)	22.5% (23/102)
Mutations on the transcribed strand	10% (2/20)	38% (11/29)
TP53 mutation pattern		
G to A	20% (4/20)	17% (5/29)
G to C	25% (5/20)	21% (6/29)
G to T	40% (8/20)	31% (9/29)
A to C	0% (0/20)	10% (3/29)
A to G	5% (1/20)	0% (0/29)
A to T	5% (1/20)	7% (2/29)
del. G/GG	5% (1/20)	14% (4/29)
TP53 mutation pattern at CpG sites		
Total G mutations at CpG	56% (10/18)	46% (11/24)
G to A at CpG	50% (2/4)	0% (0/5)
G to C at CpG	40% (2/5)	83% (5/6)
G to T at CpG	63% (5/8)	44% (4/9)
del. G/GG at CpG	100% (1/1)	50% (2/4)

control	Xpa-WT	Xpa-Null
Total 0.1% DMSO-treated HUF cultures (#)	54	54
TP53 -mutant immortalised clones (#)	2	2
Total *TP53* mutations detected (#)	2	2
Frequency of *TP53* -mutant clones	3.7% (2/54)	3.7% (2/54)
Mutations on the transcribed strand	50% (1/2)	100% (2/2)
TP53 mutation pattern		
G to A	0% (0/2)	0% (0/2)
G to C	50% (1/2)	0% (0/2)
G to T	0% (0/2)	0% (0/2)
A to C	50% (1/2)	100% (2/2)
A to G	0% (0/2)	0% (0/2)
A to T	0% (0/2)	0% (0/2)
del. G/GG	0% (0/2)	0% (0/2)
TP53 mutation pattern at CpG sites		
Total G mutations at CpG	0% (0/1)	0% (0/0)
G to A at CpG	0% (0/0)	0% (0/0)
G to C at CpG	0% (0/1)	0% (0/0)
G to T at CpG	0% (0/0)	0% (0/0)
del. G/GG at CpG	0% (0/0)	0% (0/0)

Table 2. *TP53* mutations in immortalised clones of Xpa-WT and Xpa-Null HUFs treated with BPDE and from spontaneously immortalised controls. SA = splice acceptor site; CpG indicates the presence of a mutation at a methylated CpG site; NTS = non-transcribed strand; TS = transcribed strand.

Xpa status	Clone ID*	Codon #	Exon	Mutation type	Strand	WT codon	MUT codon	Coding change	CpG	Zygosity	Contact (C), Structure (S), Zinc (Z)	Activity (Kato) **
***TP53*-mutated immortalised clones from HUFs treated with 0.5 µM BPDE**												
WT	XW-BP-91	**91**	4	G:C > A:T	NTS	TGG	TGA	W91stop		homo-/hemi-		NA
WT	XW-BP-10	**132**	5	A:T > T:A	NTS	AAG	ATG	R132M		homo-/hemi-		NF
WT	XW-BP-50	**143**	5	G:C > A:T	NTS	GTG	ATG	V143M		hetero-		NF
WT	XW-BP-83	**154**	5	G:C > T:A	NTS	GGC	GTC	G154V		hetero-		NF
WT	XW-BP-73	**158**	5	del. G	TS	CGC	_GC	frameshift	CpG	homo-/hemi-		NA
WT	XW-BP-26	**181**	5	G:C > C:G	NTS	CGC	CCC	R181P	CpG	hetero-		NF
WT	XW-BP-17	**195**	6	G:C > C:G	TS	ATC	ATG	I195M		homo-/hemi-		PF
WT	XW-BP-17	**196**	6	G:C > T:A	NTS	CGA	CTA	R196L	CpG	homo-/hemi-		PF
WT	XW-BP-2	**203**	6	G:C > T:A	NTS	GTG	TTG	V203L		hetero-		PF
WT	XW-BP-50	**213**	6	G:C > T:A	NTS	CGA	CTA	R213L	CpG	hetero-		NF
WT	XW-BP-83	**224**	6	G:C > C:G	NTS	GAG	GAC	E224D		hetero-		F
WT	XW-BP-42	**245**	7	G:C > C:G	NTS	GGC	CGC	G245R	CpG	hetero-	S	NF
WT	XW-BP-16, -55	**248**	7	G:C > A:T	NTS	CGG	CAG	R248Q	CpG	homo-/hemi-	C	NF
WT	XW-BP-95	**248**	7	G:C > T:A	NTS	CGG	CTG	R248L	CpG	hetero-	C	NF
WT	XW-BP-2	**249**	7	G:C > C:G	NTS	AGG	AGC	R249S		hetero-	S	NF
WT	XW-BP-6, -63	**273**	8	G:C > T:A	NTS	CGT	CTT	R273L	CpG	homo-/hemi-	C	NF
WT	XW-BP-9	**275**	8	G:C > T:A	NTS	TGT	TTT	C275F		homo-/hemi-		NF
WT	XW-BP-38	**286**	8	A:T > G:C	NTS	GAA	GGA	E286G		hetero-		NF
Null	XN-BP-229	**34**	4	G:C > T:A	TS	CCC	CCA	(silent) P34P		hetero-		NA
Null	XN-BP-292	**65**	4	A:T > T:A	NTS	AGA	TGA	R65stop		homo-/hemi-		NA
Null	XN-BP-201	**110**	4	G:C > C:G	NTS	CGT	CCT	R110P	CpG	hetero-		NF
Null	XN-BP-294	**127**	5	G:C > T:A	TS	TCC	TAC	S127Y		homo-/hemi-		NF
Null	XN-BP-300	**131**	5	A:T > C:G	NTS	AAC	ACC	N131T		hetero-		PF
Null	XN-BP-300	**135**	5	G:C > C:G	TS	TGC	TGG	C135W		hetero-		PF
Null	XN-BP-204	**155**	5	G:C > A:T	TS	ACC	ATC	T155I		hetero-		NF
Null	XN-BP-225	**157**	5	G:C > A:T	TS	GTC	GTT	(silent) V157V		homo-/hemi-		NA
Null	XN-BP-268	**157**	5	G:C > T:A	NTS	GTC	TTC	V157F	CpG	homo-/hemi-		NF
Null	XN-BP-225, -228	**158**	5	G:C > T:A	NTS	CGC	CTC	R158L	CpG	homo-/hemi-		NF
Null	XN-BP-238	**171**	5	G:C > T:A	NTS	GAG	TAG	E171stop		hetero-		NA
Null	XN-BP-206	**188**	6	G:C > T:A	NTS	CTG	CTT	(silent) L188L		homo-/hemi-		NA
Null	XN-BP-206	**189**	6	del. G	NTS	GCC	_CC	frameshift		homo-/hemi-		NA
Null	XN-BP-273	**196**	6	G:C > C:G	TS	CGA	GGA	R196G	CpG	homo-/hemi-		PF
Null	XN-BP-278	**211**	6	A:T > C:G	NTS	ACT	CCT	T211P		homo-/hemi-		NF
Null	XN-BP-265	**242**	7	G:C > A:T	NTS	TGC	TAC	C242Y		homo-/hemi-	Z	NF
Null	XN-BP-229	**253**	7	A:T > T:A	NTS	ACC	TCC	T253S		hetero-		PF
Null	XN-BP-299	**265**	8	A:T > C:G	TS	CTG	CGG	L265R		hetero-		NF
Null	XN-BP-296	**267**	8	del. G	NTS	CGG	C_G	frameshift	CpG	homo-/hemi-		NA
Null	XN-BP-257	**267**	8	del. GG	NTS	CGG	C__	frameshift	CpG	homo-/hemi-		NA
Null	XN-BP-210	**272**	8	G:C > A:T	NTS	GTG	ATG	V272M		hetero-		NF
Null	XN-BP-237	**273**	8	G:C > C:G	TS	CGT	GGT	R273G	CpG	homo-/hemi-	C	NF
Null	XN-BP-274	**273**	8	G:C > C:G	NTS	CGT	CCT	R273P	CpG	homo-/hemi-	C	NF
Null	XN-BP-251	**273**	8	G:C > T:A	TS	CGT	AGT	R273S	CpG	hetero-	C	NF
Null	XN-BP-254	**274**	8	G:C > T:A	NTS	GTT	TTT	V274F		homo-/hemi-		NF
Null	XN-BP-238	**282**	8	G:C > C:G	TS	CGG	GGG	R282G	CpG	hetero-	S	NF
Null	XN-BP-255	**330**	9	del. G	TS	CTT	_TT	frameshift		hetero-		NA
Null	XN-BP-204	**in. 6 (SA)**		G:C > A:T	NTS			splice		hetero-		NA
***TP53*-mutated spontaneously immortalised clones from control HUFs (treated with 0.1% DMSO)**												
WT	XW-C-115	**138**	5	G:C > C:G	NTS	GCC	CCC	A138P		homo-/hemi-		NF
WT	XW-C-137	**173**	5	A:T > C:G	TS	GTG	GGG	V173G		homo-/hemi-		NF
Null	XN-C-325	**113**	4	A:T > C:G	TS	TTC	GTC	F113V		homo-/hemi-		NF
Null	XN-C-338	**113**	4	A:T > C:G	TS	TTC	GTC	F113V		hetero-		NF

* XW = Xpa-WT; XN = Xpa-Null; BP = BPDE-treated; C = control

** The overall transactivation activity of the mutant in a yeast functional assay published by Kato *et al.* [50]. (NF = non-functional, PF = partially functional, F = functional, NA = not assessed)

Legends to Figures

Figure 1. DNA adduct formation in Xpa-WT and Xpa-Null Hupki mice treated with BaP. Mice were treated with BaP (125 or 12.5 mg/kg bw) as indicated; (A) and (C) were treated once, (B) and (D) were treated once a day for 5 days. DNA adduct levels in different tissues were assessed by ^{32}P-postlabelling. Values represent means ± SD from 3 animals, and each DNA sample was measured by two independent ^{32}P-postlabelling analyses. ND = not detected; † = not determined due to death of Xpa-Null animals. See Fig. S3 for representative autoradiograms showing the adduct profiles in the different tissues examined. Statistical analysis, comparing adduct levels in tissues from Xpa-WT and Xpa-Null mice, was performed using the Student's *t*-test; * $P < 0.05$, ** $P < 0.01$, *** $P < 0.001$.

Figure 2. Growth and BaP-induced DNA adduct formation in HUFs cultured at 20% or 3% O_2. (A) and (B): Xpa-WT or Xpa-Null HUFs (2.5×10^5 cells/ 25-cm^2 flask) were cultured for up to 50 days in 20% O_2 (A) or 3% O_2 (B). Cells were counted every 3–4 days, diluted and reseeded to determine the cumulative population doublings over time. (C): Xpa-WT HUFs cultured at 20% or 3% O_2 were treated for 24 or 48 hr with 1 μM BaP. DNA adduct levels were assessed by ^{32}P-postlabelling. Values represent means ± SD of two biological replicates where each DNA sample was measured by two independent ^{32}P-postlabelling analyses.

Figure 3. Survival of Xpa-WT and Xpa-Null HUFs and DNA adduct formation following treatment with BaP or BPDE. (A) and (B) Cells were treated with the indicated doses of BaP (24 or 48 hr) or BPDE (2 hr); survival was measured at 24 or 48 hr following initiation of treatment using a crystal violet staining assay. Cells treated with 0.1% DMSO served as solvent control. Mean values are shown as % of control ± SD of 5 replicate wells. The data are representative of at least three independent experiments (variation ≤ 15%). (C) and (D) Cells were treated with the indicated doses of BaP (24 hr) or BPDE (2 hr). DNA adduct levels were assessed by ^{32}P-postlabelling. Values represent means ± SD of two biological replicates where each DNA sample was measured by two independent ^{32}P-postlabelling analyses. Statistical analysis, comparing DNA adduct levels in Xpa-WT and Xpa-Null HUFs, was performed by 2-factor ANOVA followed by Bonferroni's post-hoc contrasts; * $P < 0.05$. Inserts: Autoradiographic profiles of DNA adducts obtained in HUFs treated with BaP, as indicated; the origins, in the bottom left-hand corner, were cut off before exposure; arrow shows 10-(deoxyguanosin-N^2-yl)-7,8,9-trihydroxy-7,8,9,10-tetrahydrobenzo[*a*]pyrene (BPDE-N^2-dG).

Figure 4. The pattern and strand bias of *TP53* mutations in immortalised clones of Xpa-WT and Xpa-Null HUFs treated with BPDE. (A) The percentage of each type of single base substitution or deletion is shown. (B) The number of each type of single base substitution or deletion occurring on the non-transcribed strand (NTS) or transcribed strand (TS) is shown.

Figure 5. The codon distribution of *TP53* mutations induced by BPDE in Xpa-WT and Xpa-Null HUFs compared with the spectrum found in human tumours. Shown are (A) the number of mutations at each codon (within exons 4–9) in the *TP53* gene induced by BPDE in HUFs compared with the frequency of mutation at each codon in (B) lung cancer of smokers (exclusions: radon, asbestos, mustard gas, and coal [74, 75]), (C) lung cancer of non- and passive-smokers (exclusions: radon, asbestos, mustard gas, and coal [74, 75]) and (D) cancer overall. Reference for

human cancer mutation codon distribution: IARC TP53 Mutation Database, R17 (November 2013). Mutation hotspots are indicated in grey.

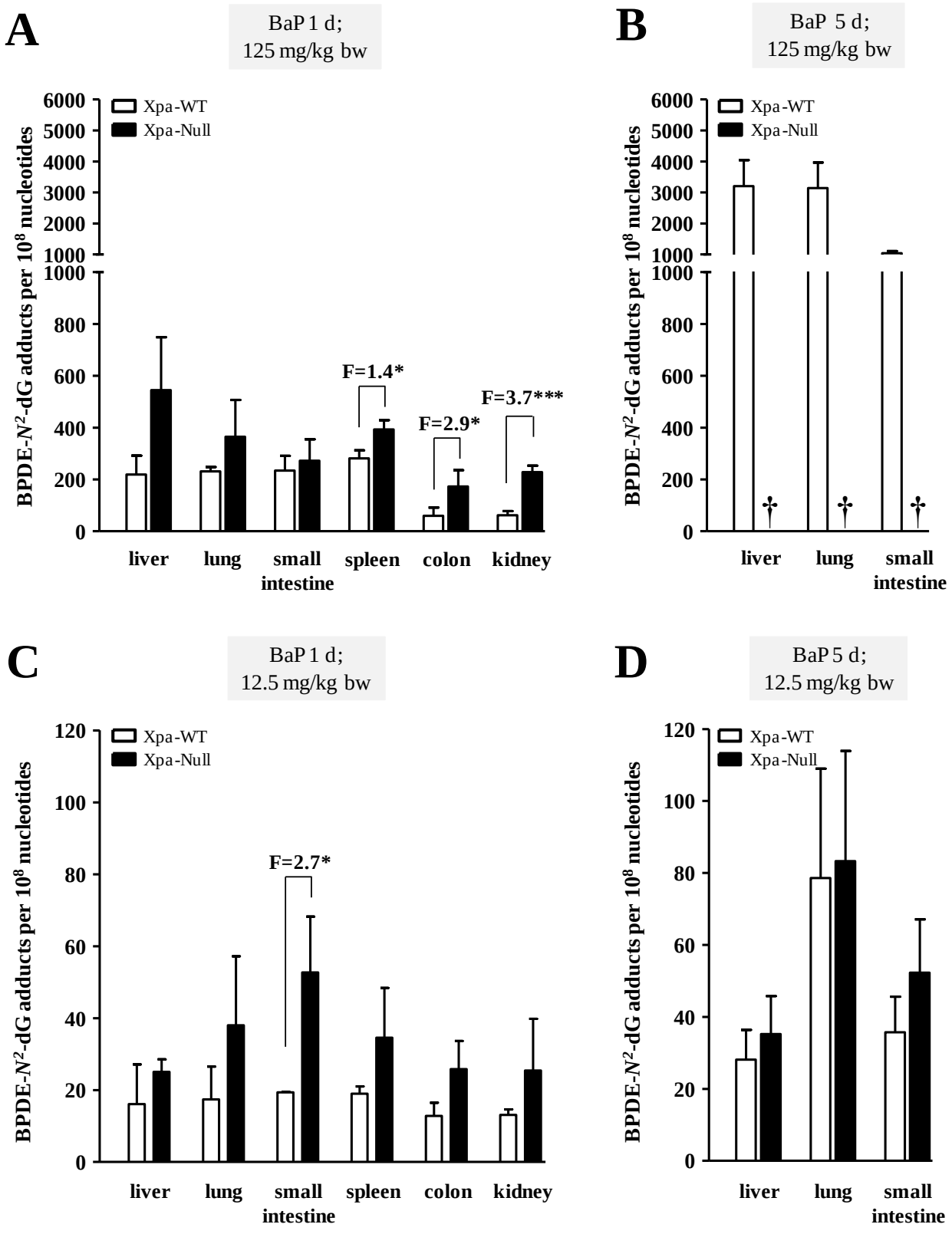
A
BaP 1 d;
125 mg/kg bw
Xpa-WT
Xpa-Null
BPDE-N2-dG adducts per 10^8 nucleotides
F=1.4*
F=2.9*
F=3.7***
liver
lung
small intestine
spleen
colon
kidney
B
BaP 5 d;
125 mg/kg bw
C
BaP 1 d;
12.5 mg/kg bw
F=2.7*
D
BaP 5 d;
12.5 mg/kg bw

Figure 1.

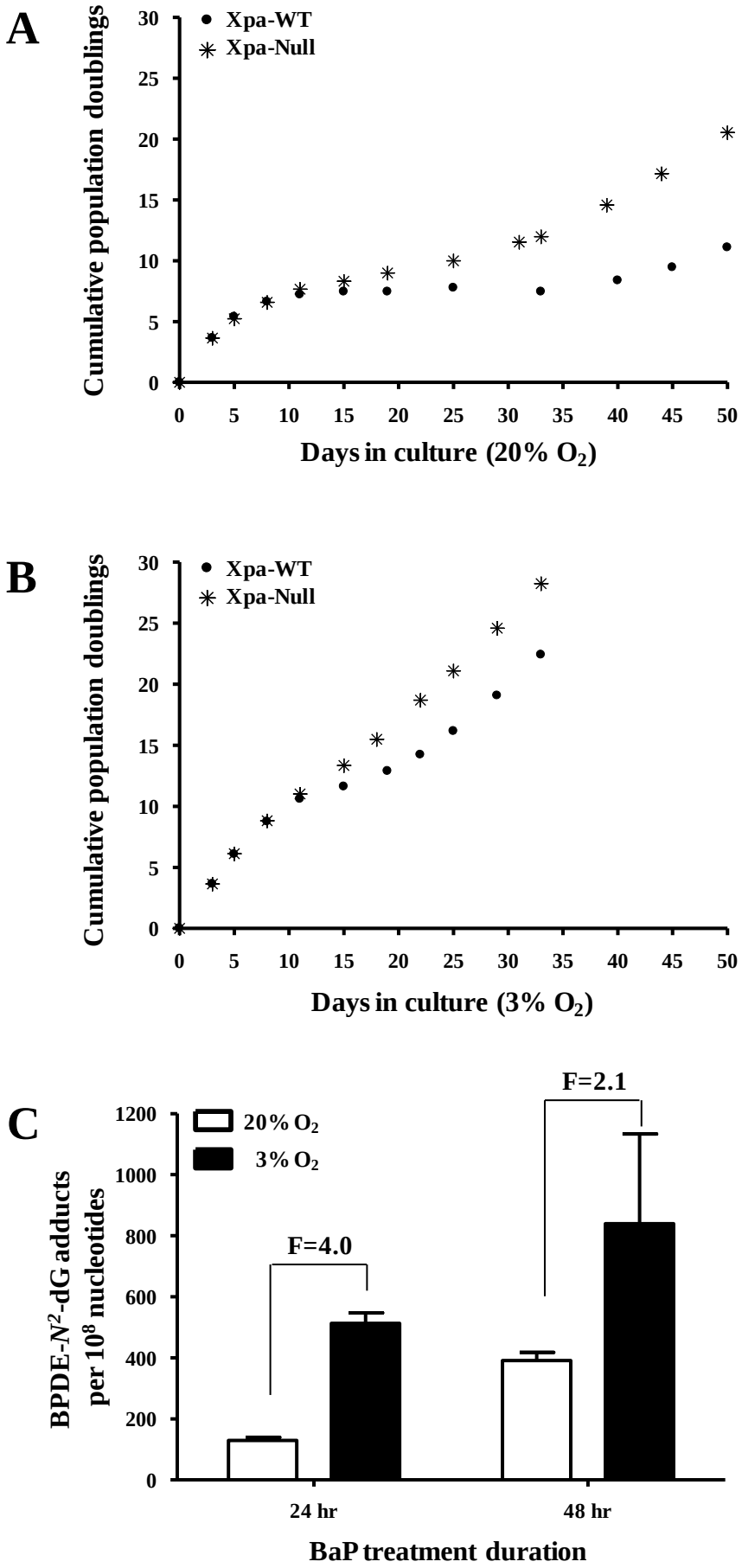
A
Xpa-WT
Xpa-Null
Cumulative population doublings
Days in culture (20% O2)
B
Xpa-WT
Xpa-Null
Cumulative population doublings
Days in culture (3% O2)
C
20% O2
3% O2
F=4.0
F=2.1
BPDE-N2-dG adducts per 10^8 nucleotides
24 hr
48 hr
BaP treatment duration

Figure 2.

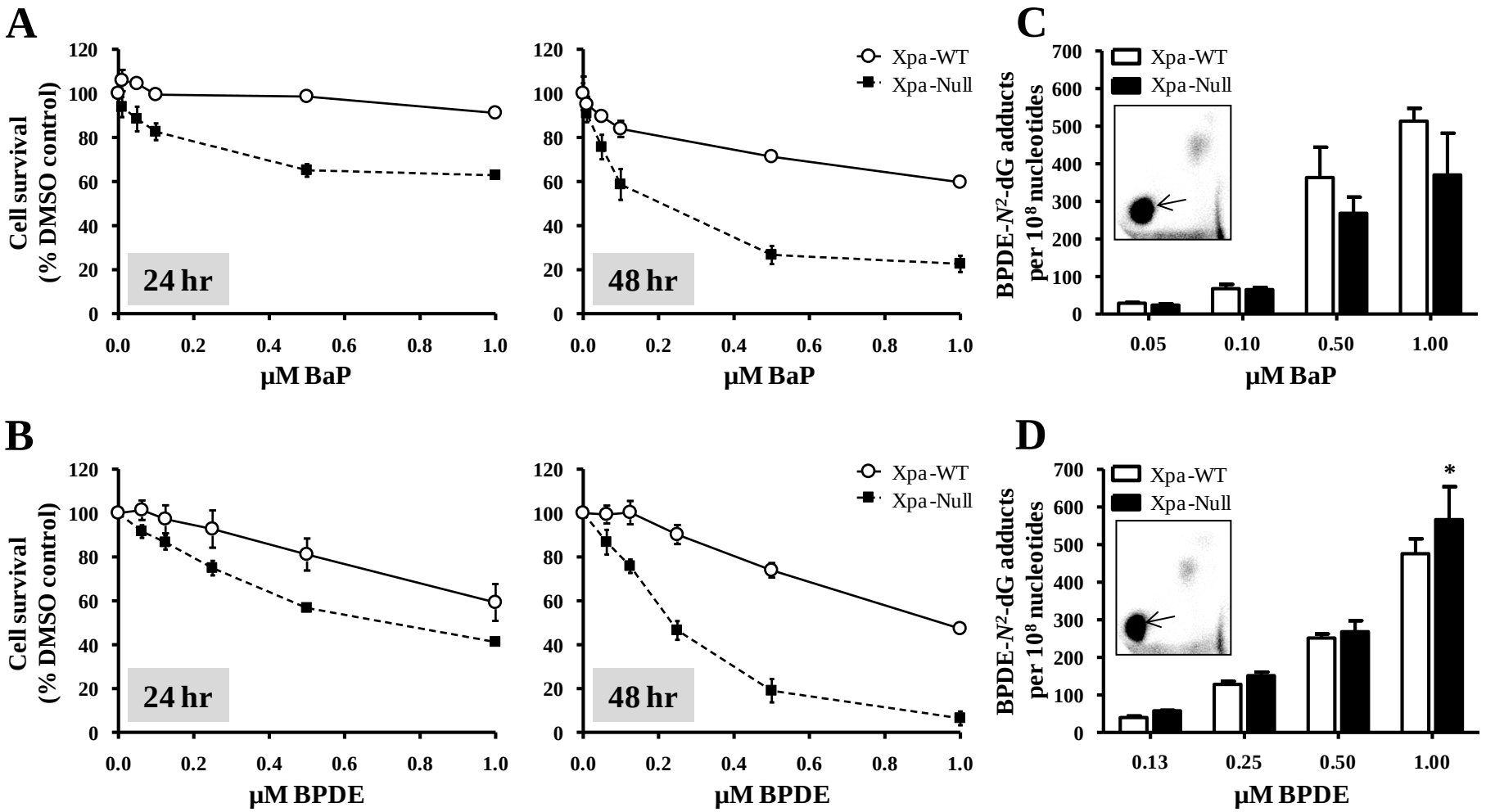
A
Cell survival (% DMSO control)
24 hr
48 hr
μM BaP
Xpa-WT
Xpa-Null
B
μM BPDE
C
BPDE-N2-dG adducts per 10^8 nucleotides
0.05
0.10
0.50
1.00
D
*
0.13
0.25
0.50
1.00

Figure 3.

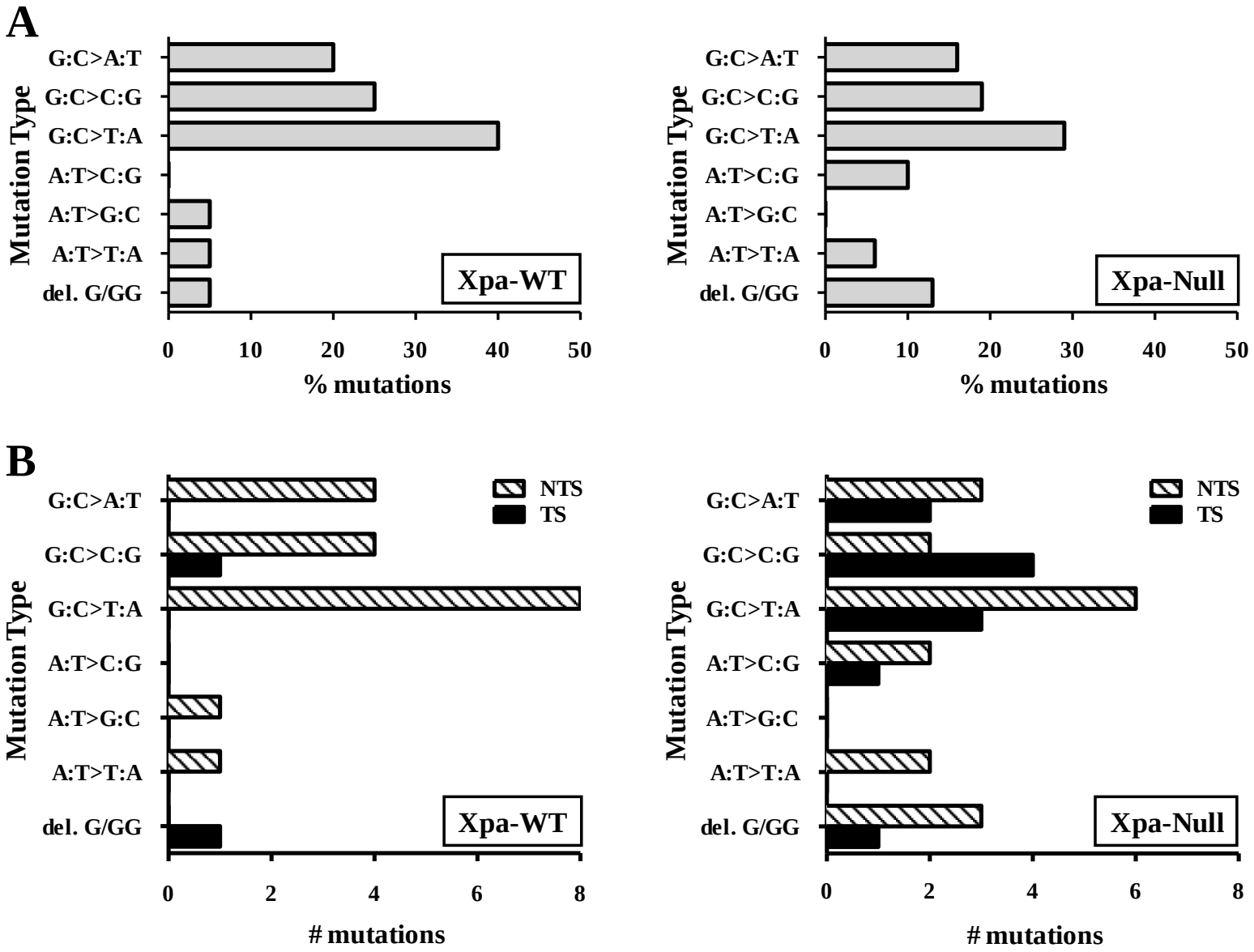
A
Mutation Type
G:C>A:T
G:C>C:G
G:C>T:A
A:T>C:G
A:T>G:C
A:T>T:A
del. G/GG
Xpa-WT
0
10
20
30
40
50
% mutations
Xpa-Null
B
NTS
TS
mutations
0
2
4
6
8

Figure 4.

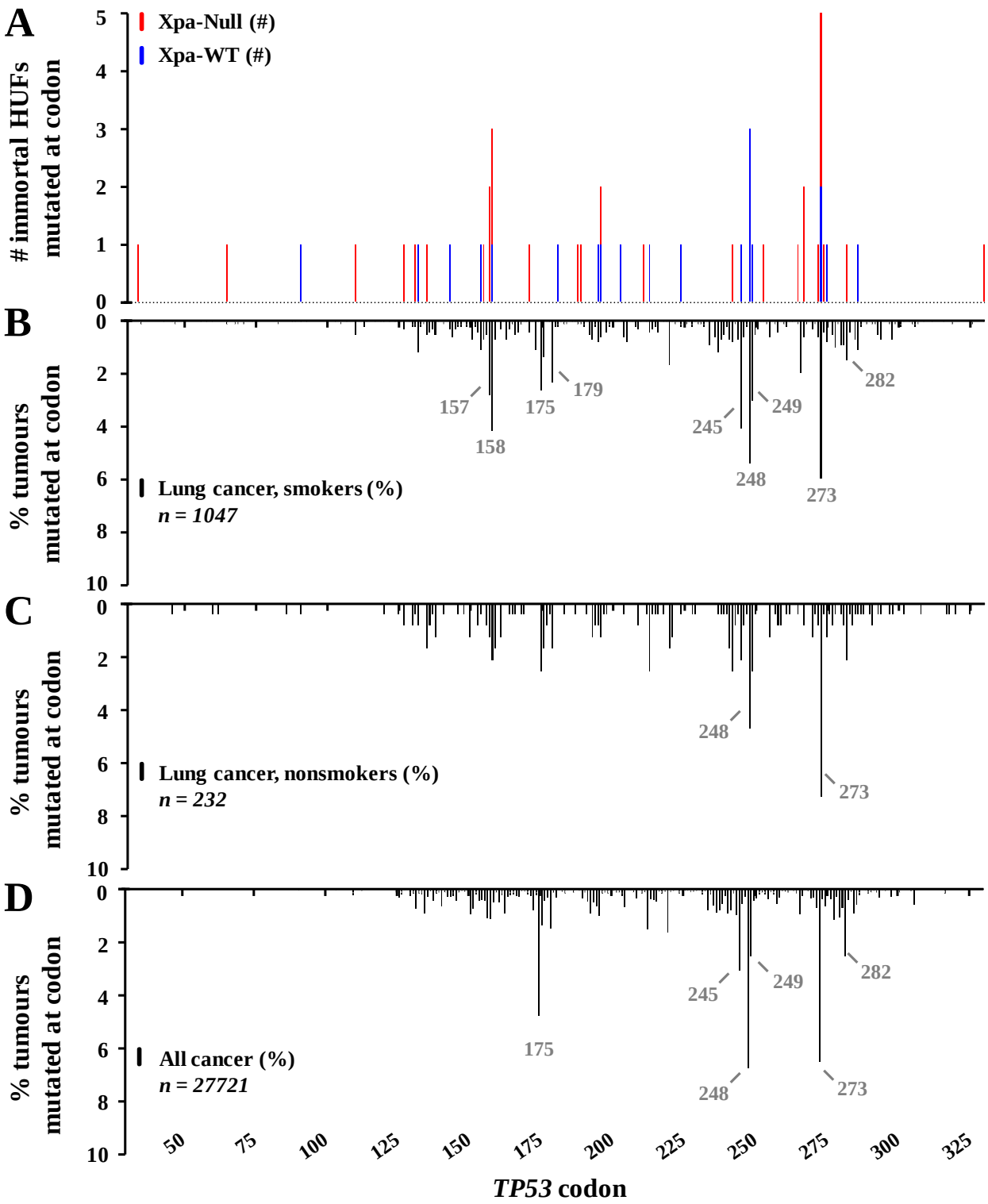
A
immortal HUFs mutated at codon
Xpa-Null (#)
Xpa-WT (#)
B
% tumours mutated at codon
Lung cancer, smokers (%)
n = 1047
157
158
175
179
245
248
249
273
282
C
% tumours mutated at codon
Lung cancer, nonsmokers (%)
n = 232
248
273
D
% tumours mutated at codon
All cancer (%)
n = 27721
175
245
248
249
273
282
50
75
100
125
150
175
200
225
250
275
300
325
TP53 codon

Figure 5.

Supplementary Tables and Figures

Table S1. Primer sequences and PCR conditions for genotyping *Hupki*, mouse *Trp53*, WT *Xpa* and *Xpa*-knockout alleles.

Allele	Primer Name	Primer sequence	Primer details
Hupki	IMR1732	5' GCC TCA TCT TGG GCC TGT GTT ATC TCC 3'	Forward primer for *Hupki* allele
	IMR1733	5' GGC CAG TGT GCA GGG TGG CAA GTG GCT C 3'	Reverse primer for *Hupki* allele
wild-type *Trp53*	IMR1734	5' ACT CCA TGG CCC CTG TCA TC 3'	Forward primer for wild-type mouse *Trp53* allele
	IMR1735	5' AGG TCA CAC GAA AGA CAA CT 3'	Reverse primer for wild-type mouse *Trp53* allele
Xpa	XP26	5' GTG TCA GGC ATA AGA TCT ATG ACAA 3'	Forward primer in intron 2 of *Xpa* gene
	XP47	5' AGG CAA GCA CCT GCA GCT GT 3'	Reverse primer spanning intron 3 and exon 3 of *Xpa* gene
	PGK2	5' GGC CAC TTG TGT AGC GCC AA 3'	Reverse primer in PGK2 promoter of Neo-resistance cassette

Hupki **PCR reaction components**	**Volume per reaction**	**Final concentration per reaction**	**Cycling parameters**			**Product size**
RedTaq 2X Ready Mix (Sigma #R2523)	6.25 µL	1X	94°C	1.5 minutes	1 cycle	*Hupki* : 172 bp
IMR1732 (H) primer [10 µM]	0.5 µL	5 pmol	94°C	30 seconds	35 cycles	
IMR1733 (H) primer [10 µM]	0.5 µL	5 pmol	66°C	1 minute		
Ear clip DNA extract	2 µL		72°C	2 minutes		
nuclease-free water	3.25 µL		72°C	2 minutes	1 cycle	
final volume of 12.5 µL			4 - 10°C	Hold		

mouse *Trp53* **PCR reaction components**	**Volume per reaction**	**Final concentration per reaction**	**Cycling parameters**			**Product size**
RedTaq 2X Ready Mix (Sigma #R2523)	6.25 µL	1X	94°C	1.5 minutes	1 cycle	mouse *Trp53* : 146 bp
IMR1734 (M) primer [10 µM]	0.5 µL	5 pmol	94°C	30 seconds	35 cycles	
IMR1735 (M) primer [10 µM]	0.5 µL	5 pmol	66°C	1 minute		
Ear clip DNA extract	2 µL		72°C	2 minutes		
nuclease-free water	3.25 µL		72°C	2 minutes	1 cycle	
final volume of 12.5 µL			4 - 10°C	Hold		

Xpa **PCR reaction components**	**Volume per reaction**	**Final concentration per reaction**	**Cycling parameters**			**Product size**
RedTaq 2X Ready Mix (Sigma #R2523)	6.25 µL	1X	94°C	1 minute	35 cycles	WT *Xpa* : 214 bp Null *Xpa* : 132 bp
XP26 primer [10 µM]	1.0 µL	10 pmol	60°C	1 minute		
XP47 primer [10 µM]	0.5 µL	5 pmol	70°C	2 minutes		
PGK2 primer [10 µM]	0.5 µL	5 pmol	72°C	10 minutes	1 cycle	
Ear clip DNA extract	2 µL		4 - 10°C	Hold		
nuclease-free water	2.25 µL					
final volume of 12.5 µL						

Table S2. Primer sequences, PCR conditions and reference sequences for DNA sequencing exons 4–9 of Hupki *TP53*. For C: intronic sequence is lower case, exonic sequence is upper case, and primer binding sites are bold/underlined.

A. Primer Information

TP53 Exon(s)	Primer Name	Forward /Reverse	Primer sequence 5' > 3'	Reaction
Exon 4	GCEx4F	Forward	GTC CTC TGA CTG CTC TTT TCA CCC ATC TAC	PCR
	GCEx4R	Reverse	GGG ATA CGG CCA GGC ATT GAA GTC TC	PCR
	HUPKI4RJ2	Reverse	GAT ACG GCC AGG CAT TG	sequencing
Exons 5 & 6	GCEx5F	Forward	CTT GTG CCC TGA CTT TCA ACT CTG TCT C	PCR
	GCEx6R	Reverse	GCC ACT GAC AAC CAC CCT TAA CCC CTC	PCR
	HUPKI6RJ2	Reverse	GCC ACT GAC AAC CAC C	sequencing
Exon 7	p53ex7F MH08	Forward	AGA TCA CGC CAC TGC ACT C	PCR
	p53ex7R MH08	Reverse	CCG GAA ATG TGA TGA GAG GT	PCR & sequencing
Exons 8 & 9	p53ex8F MH08	Forward	CAA GGG TGG TTG GGA GTA GA	PCR & sequencing
	p53ex9R MH08	Reverse	GTC TCT GGC ATG CGA CTC TC	PCR

B. PCR amplification

PCR reaction components (all exons)	Volume per reaction	Final concentration per reaction	Cycling parameters		
2X Ready Mix with Taq (Sigma #P4600)	12.5 µL	1X	94°C	4 minutes	1 cycle
Forward primer (10 µM stock)	2.0 µL	20 pmol	94°C	30 seconds	40 cycles
Reverse primer	2.0 µL	20 pmol	60°C	30 seconds	
DNA (100 ng/µL)	2.0 µL	200 ng	72°C	1 minute	
nuclease-free water	6.5 µL		72°C	7 minutes	1 cycle
			4 - 10°C	Hold	

Expected products			
Exon 4	366 bp	Exon 7	376 bp
Exon 5 - 6	478 bp	Exon 8 - 9	498 bp

C. Reference sequences for PCR Amplicons

Exon 4

gtcctctgactgctcttttcacccatctacagTCCCCCTTGCCGTCCCAAGCAATGGATGATTTGATGCTGTCCCCGGACGATATTGAACAATGGT
TCACTGAAGACCCAGGTCCAGATGAAGCTCCCAGAATGCCAGAGGCTGCTCCCCCCGTGGCCCCTGCACCAGCAGCTCCTACA
CCGGCGGCCCCTGCACCAGCCCCCTCCTGGCCCCTGTCATCTTCTGTCCCTTCCCAGAAAACCTACCAGGGCAGCTACGGTTTC
CGTCTGGGCTTCTTGCATTCTGGGACAGCCAAGTCTGTGACTTGCACGgtcagttgccctgaggggctggcttccat**gagacttcaatgcctggccgtatccc**

Exon 5 - 6

cttgtgccctgactttcaactctgtctccttcctcttcctacagTACTCCCCTGCCCTCAACAAGATGTTTTGCCAACTGGCCAAGACCTGCCCTGTGCAG
CTGTGGGTTGATTCCACACCCCCGCCCGGCACCCGCGTCCGCGCCATGGCCATCTACAAGCAGTCACAGCACATGACGGAGGT
TGTGAGGCGCTGCCCCCACCATGAGCGCTGCTCAGATAGCGATGgtgagcagctggggctggagagacgacagggctggttgcccagggtccccaggcctctga
ttcctcactgattgctcttagGTCTGGCCCCTCCTCAGCATCTTATCCGAGTGGAAGGAAATTTGCGTGTGGAGTATTTGGATGACAGAAAC
ACTTTTCGACATAGTGTGGTGGTGCCCTATGAGCCGCCTGAGgtctggtttgcaactggggtctctgggag**gaggggttaagggtggttgtcagtggc**

Exon 7

agatcacgccactgcactccagcctgggcgacagagcgagattccatctcaaaaaaaaaaaaaaaggcctcccctgcttgccacaggtctccccaaggcgcactggcctcatcttgggcctgtgttatctc
ctagGTTGGCTCTGACTGTACCACCATCCACTACAACTACATGTGTAACAGTTCCTGCATGGGCGGCATGAACCGGAGGCCCATC
CTCACCATCATCACACTGGAAGACTCCAGgtcaggagccacttgccaccctgcacactggcctgctgtgccccagcctctgcttgcctctgaccccctgggcccacctcttaccgatt
tcttccatactactacccatcc**acctctcatcacatttccgg**

Exon 8 - 9

caagggtggttgggagtagatggagcctggttttttaaatgggacaggtaggacctgatttccttactgcctcttgcttctctttttcctatcctgagtagTGGTAATCTACTGGGACGGAACA
GCTTTGAGGTGCGTGTTTGTGCCTGTCCTGGGAGAGACCGGCGCACAGAGGAAGAGAATCTCCGCAAGAAAGGGGAGCCTCA
CCACGAGCTGCCCCCAGGGAGCACTAAGCGAGgtaagcaagcaggacaagaagcggtggaggagaccaagggtgcagttatgcctcagattcacttttatcacctttccttgcc
tctttcctagCACTGCCCAACAACACCAGCTCCTCTCCCCAGCCAAAGAAGAAACCACTGGATGGAGAATATTTCACCCTTCAGgtacta
agtcttgggacctcttatcaagtggaaagtttccagtctaacactcaaaatgccgt <*human seq, mouse seq*> ggtaccaaggctg**gagagtcgcatgccagagac**

Table S3. Sequence context of *TP53* mutations induced by BPDE in HUFs. For each type of single base substitution or deletion, the 5' and 3' base are shown. SA = splice acceptor site; CpG indicates the presence of a mutation at a methylated CpG site; NTS = nontranscribed strand; TS = transcribed strand. DNA strand indicates the strand of the G or A substitution.

Clone ID*	Xpa Status	Codon	WT codon (NTS)	MUT codon (NTS)	DNA strand	CpG site	G or A substitution	5' base	3' base	Coding Description
XN-BP-300	Null	**131**	AAC	ACC	NTS		A:T > C:G	A	C	c.392A>C
XN-BP-278	Null	**211**	ACT	CCT	NTS		A:T > C:G	C	C	c.631A>C
XN-BP-299	Null	**265**	CTG	CGG	TS		A:T > C:G	C	G	c.794T>G
XW-BP-38	WT	**286**	GAA	GGA	NTS		A:T > G:C	G	A	c.857A>G
XW-BP-10	WT	**132**	AAG	ATG	NTS		A:T > T:A	A	G	c.395A>T
XN-BP-229	Null	**253**	ACC	TCC	NTS		A:T > T:A	C	C	c.757A>T
XN-BP-292	Null	**65**	AGA	TGA	NTS		A:T > T:A	C	G	c.193A>T
XN-BP-255	Null	**330**	CTT	_TT	TS		del. G	A	G	c.988del1
XW-BP-73	WT	**158**	CGC	_GC	TS	**CpG**	del. G	C	G	c.472del1
XN-BP-296	Null	**267**	CGG	C_G	NTS	**CpG**	del. G	C	G	c.800del1
XN-BP-206	Null	**189**	GCC	_CC	NTS		del. G	G	C	c.565del1
XN-BP-257	Null	**267**	CGG	C__	NTS	**CpG**	del. GG	C	A	c.800del2
XN-BP-204	Null	**in. 6 (SA)**			NTS		G:C > A:T	A	G	c.673-1G>A
XW-BP-16	WT	**248**	CGG	CAG	NTS	**CpG**	G:C > A:T	C	G	c.743G>A
XW-BP-55	WT	**248**	CGG	CAG	NTS	**CpG**	G:C > A:T	C	G	c.743G>A
XN-BP-225	Null	**157**	GTC	GTT	TS		G:C > A:T	G	A	c.471C>T
XW-BP-91	WT	**91**	TGG	TGA	NTS		G:C > A:T	G	C	c.273G>A
XN-BP-204	Null	**155**	ACC	ATC	TS		G:C > A:T	G	T	c.464C>T
XN-BP-210	Null	**272**	GTG	ATG	NTS		G:C > A:T	G	T	c.814G>A
XN-BP-265	Null	**242**	TGC	TAC	NTS		G:C > A:T	T	C	c.725G>A
XW-BP-50	WT	**143**	GTG	ATG	NTS		G:C > A:T	T	T	c.427G>A
XW-BP-83	WT	**224**	GAG	GAC	NTS		G:C > C:G	A	G	c.672G>C
XW-BP-26	WT	**181**	CGC	CCC	NTS	**CpG**	G:C > C:G	C	C	c.542G>C
XN-BP-237	Null	**273**	CGT	GGT	TS	**CpG**	G:C > C:G	C	C	c.817C>G
XN-BP-273	Null	**196**	CGA	GGA	TS	**CpG**	G:C > C:G	C	G	c.586C>G
XW-BP-42	WT	**245**	GGC	CGC	NTS	**CpG**	G:C > C:G	C	G	c.733G>C
XN-BP-238	Null	**282**	CGG	GGG	TS	**CpG**	G:C > C:G	C	G	c.844C>G
XN-BP-201	Null	**110**	CGT	CCT	NTS	**CpG**	G:C > C:G	C	T	c.329G>C
XN-BP-274	Null	**273**	CGT	CCT	NTS	**CpG**	G:C > C:G	C	T	c.818G>C
XW-BP-17	WT	**195**	ATC	ATG	TS		G:C > C:G	G	A	c.585C>G
XN-BP-300	Null	**135**	TGC	TGG	TS		G:C > C:G	G	C	c.405C>G
XW-BP-2	WT	**249**	AGG	AGC	NTS		G:C > C:G	G	C	c.747G>C
XN-BP-229	Null	**34**	CCC	CCA	TS		G:C > T:A	A	G	c.102C>A
XW-BP-17	WT	**196**	CGA	CTA	NTS	**CpG**	G:C > T:A	C	A	c.587G>T
XW-BP-50	WT	**213**	CGA	CTA	NTS	**CpG**	G:C > T:A	C	A	c.638G>T
XN-BP-225	Null	**158**	CGC	CTC	NTS	**CpG**	G:C > T:A	C	C	c.473G>T
XN-BP-228	Null	**158**	CGC	CTC	NTS	**CpG**	G:C > T:A	C	C	c.473G>T
XN-BP-251	Null	**273**	CGT	AGT	TS	**CpG**	G:C > T:A	C	C	c.817C>A
XW-BP-95	WT	**248**	CGG	CTG	NTS	**CpG**	G:C > T:A	C	G	c.743G>T
XN-BP-268	Null	**157**	GTC	TTC	NTS	**CpG**	G:C > T:A	C	T	c.469G>T
XW-BP-6	WT	**273**	CGT	CTT	NTS	**CpG**	G:C > T:A	C	T	c.818G>T
XW-BP-63	WT	**273**	CGT	CTT	NTS	**CpG**	G:C > T:A	C	T	c.818G>T
XN-BP-294	Null	**127**	TCC	TAC	TS		G:C > T:A	G	A	c.380C>A
XN-BP-238	Null	**171**	GAG	TAG	NTS		G:C > T:A	G	A	c.511G>T
XW-BP-83	WT	**154**	GGC	GTC	NTS		G:C > T:A	G	C	c.461G>T
XN-BP-206	Null	**188**	CTG	CTT	NTS		G:C > T:A	T	G	c.564G>T
XW-BP-2	WT	**203**	GTG	TTG	NTS		G:C > T:A	T	T	c.607G>T
XN-BP-254	Null	**274**	GTT	TTT	NTS		G:C > T:A	T	T	c.820G>T
XW-BP-9	WT	**275**	TGT	TTT	NTS		G:C > T:A	T	T	c.824G>T

* XW = Xpa-WT; XN = Xpa-Null; BP = BPDE-treated; C = control

Table S4. The occurrence in human cancer of *TP53* mutations found in BPDE-treated HUFs.

Clone ID*	Coding Description	Coding change	Codon #	# of tumours harbouring mutation (codon) **			CpG
				Lung cancer, smokers***	Lung cancer, non-smokers****	All cancer	
XN-BP-229	c.102C>A	(silent) P34P	**34**	0 (0)	0 (0)	0 (4)	
XN-BP-292	c.193A>T	R65stop	**65**	2 (2)	0 (0)	4 (6)	
XW-BP-91	c.273G>A	W91stop	**91**	0 (1)	0 (1)	12 (30)	
XN-BP-201	c.329G>C	R110P	**110**	1 (6)	0 (0)	15 (76)	CpG
XN-BP-294	c.380C>A	S127Y	**127**	1 (4)	0 (2)	11 (66)	
XN-BP-300	c.392A>C	N131T	**131**	0 (3)	0 (1)	0 (62)	
XW-BP-10	c.395A>T	R132M	**132**	1 (13)	0 (2)	14 (217)	
XN-BP-300	c.405C>G	C135W	**135**	2 (6)	1 (4)	28 (267)	
XW-BP-50	c.427G>A	V143M	**143**	1 (4)	0 (0)	35 (96)	
XW-BP-83	c.461G>T	G154V	**154**	7 (12)	1 (1)	67 (129)	
XN-BP-204	c.464C>T	T155I	**155**	2 (8)	0 (0)	21 (128)	
XN-BP-268	c.469G>T	V157F	**157**	24 (30)	1 (3)	210 (313)	CpG
XN-BP-225	c.471C>T	(silent) V157V	**157**	0 (30)	0 (3)	5 (313)	
XW-BP-73	c.472del1	frameshift	**158**	1 (44)	0 (5)	8 (326)	CpG
XN-BP-225, -228	c.473G>T	R158L	**158**	32 (44)	1 (5)	102 (326)	CpG
XN-BP-238	c.511G>T	E171stop	**171**	3 (5)	0 (0)	22 (65)	
XW-BP-26	c.542G>C	R181P	**181**	2 (3)	0 (0)	24 (106)	CpG
XN-BP-206	c.564G>T	(silent) L188L	**188**	0 (2)	0 (0)	0 (14)	
XN-BP-206	c.565del1	frameshift	**189**	1 (2)	0 (0)	2 (34)	
XW-BP-17	c.585C>G	I195M	**195**	0 (9)	0 (2)	0 (196)	
XW-BP-17	c.587G>T	R196L	**196**	0 (7)	0 (3)	2 (289)	CpG
XN-BP-273	c.586C>G	R196G	**196**	0 (7)	1 (3)	3 (289)	CpG
XW-BP-2	c.607G>T	V203L	**203**	0 (0)	0 (0)	8 (49)	
XN-BP-278	c.631A>C	T211P	**211**	0 (0)	0 (0)	1 (59)	
XW-BP-50	c.638G>T	R213L	**213**	1 (5)	1 (6)	41 (435)	CpG
XW-BP-83	c.672G>C	E224D	**224**	0 (3)	0 (1)	9 (58)	
XN-BP-265	c.725G>A	C242Y	**242**	3 (9)	2 (6)	56 (237)	
XW-BP-42	c.733G>C	G245R	**245**	5 (43)	2 (5)	19 (866)	CpG
XW-BP-16, -55	c.743G>A	R248Q	**248**	15 (56)	6 (11)	933 (1880)	CpG
XW-BP-95	c.743G>T	R248L	**248**	23 (56)	1 (11)	121 (1880)	CpG
XW-BP-2	c.747G>C	R249S	**249**	0 (32)	0 (6)	42 (719)	
XN-BP-229	c.757A>T	T253S	**253**	0 (1)	0 (0)	5 (49)	
XN-BP-299	c.794T>G	L265R	**265**	0 (1)	0 (1)	5 (58)	
XN-BP-296	c.800del1	frameshift	**267**	0 (7)	0 (2)	3 (86)	CpG
XN-BP-257	c.800del2	frameshift	**267**	0 (7)	0 (2)	0 (86)	CpG
XN-BP-210	c.814G>A	V272M	**272**	3 (7)	1 (2)	114 (211)	
XN-BP-237	c.817C>G	R273G	**273**	3 (62)	0 (17)	19 (1814)	CpG
XN-BP-251	c.817C>A	R273S	**273**	3 (62)	0 (17)	19 (1814)	CpG
XW-BP-6, -63	c.818G>T	R273L	**273**	30 (62)	4 (17)	155 (1814)	CpG
XN-BP-274	c.818G>C	R273P	**273**	2 (62)	0 (17)	38 (1814)	CpG
XN-BP-254	c.820G>T	V274F	**274**	3 (5)	1 (1)	34 (118)	
XW-BP-9	c.824G>T	C275F	**275**	4 (9)	1 (3)	54 (193)	
XN-BP-238	c.844C>G	R282G	**282**	2 (16)	0 (5)	48 (715)	CpG
XW-BP-38	c.857A>G	E286G	**286**	1 (12)	0 (1)	20 (176)	
XN-BP-255	c.988del1	frameshift	**330**	0 (1)	0 (0)	1 (13)	
XN-BP-204	c.673-1G>A	splice	**in. 6**	0 (6)	0 (0)	12 (69)	

* XW = Xpa-WT; XN = Xpa-Null; BP = BPDE-treated; C = control; ** Reference data: IARC TP53 Mutation Database, R17 (November 2013). *** Lung cancer in smokers (exclusions: radon, asbestos, mustard gas, and coal [3, 4]; **** Lung cancer in non- and passive-smokers (exclusions: radon, asbestos, mustard gas, and coal [3, 4].

Table S5. Comparison of *TP53* mutations generated in the current study with mutations identified in all previous HIMAs. Exact mutation matches, as well as codons mutated in previous HIMAs, are indicated with an 'x' and are also in bold. The number of HUF cell lines in which a mutation previously occurred is shown. 3-NBA = 3-nitrobenzanthrone; BaP = benzo[*a*]pyrene; AAI = aristolochic acid I; UV = ultraviolet irradiation; MNNG: 1-methyl-2-nitro-1-nitrosoguanidine; control = spontaneously immortalised, untreated.

Treatment	WT codon	Mutant codon	Base change	Codon	Occurrence: HUF cell lines	Reference	Codon mutated in current study	Mutation match with current study
3-NBA	CGC	CGA	G:C>T:A	72	1	vom Brocke 2009		
3-NBA	CCT	CAT	G:C>T:A	128	1	vom Brocke 2009		
3-NBA	TAC	TGC	A:T>G:C	163	4	vom Brocke 2009		
3-NBA	GTG	TTG	G:C>T:A	173	1	vom Brocke 2009		
3-NBA	TGC	TGG	G:C>C:G	176	1	vom Brocke 2009		
3-NBA	ATC	TTC	A:T>T:A	**195**	1	vom Brocke 2009	x	
3-NBA	**CGA**	**CTA**	**G:C>T:A**	**196**	**1**	vom Brocke 2009	x	x
3-NBA	TAT	AAT	A:T>T:A	205	1	vom Brocke 2009		
3-NBA	TTG	GTG	A:T>C:G	206	1	vom Brocke 2009		
3-NBA	TAC	TGC	A:T>G:C	236	2	vom Brocke 2009		
3-NBA	GGC	GCC	G:C>C:G	244	2	vom Brocke 2009		
3-NBA	GGC	GCC	G:C>C:G	**245**	2	vom Brocke 2009	x	
3-NBA	ATG	AAG	A:T>T:A	246	1	vom Brocke 2009		
3-NBA	AAC	ACC	A:T>C:G	247	1	vom Brocke 2009		
3-NBA	ACA	AAA	G:C>T:A	256	1	vom Brocke 2009		
3-NBA	TTT	GTT	A:T>C:G	270	1	vom Brocke 2009		
3-NBA	**CGT**	**CTT**	**G:C>T:A**	**273**	**1**	vom Brocke 2009	x	x
3-NBA	**GTT**	**TTT**	**G:C>T:A**	**274**	**2**	vom Brocke 2009	x	x
3-NBA	AGA	ATA	G:C>T:A	280	1	vom Brocke 2009		
BaP	GGG	TGG	G:C>T:A	117	1	Liu 2005		
BaP	GCC	GGC	G:C>C:G	119	1	Reinbold 2007		
BaP	**TGC**	**TGG**	**G:C>C:G**	**135**	**1**	Reinbold 2007	x	x
BaP	GCC	GGC	G:C>C:G	138	1	Liu 2005		
BaP	TGC	TGG	G:C>C:G	141	1	Reinbold 2007		
BaP	CAG	CAT	G:C>T:A	144	1	Reinbold 2007		
BaP	**GTC**	**GTT**	**G:C>A:T**	**157**	**2**	Liu 2005	x	x
BaP	**GTC**	**TTC**	**G:C>T:A**	**157**	**3**	Liu 2005, Reinbold 2007	x	x
BaP	CGC	CCC	G:C>C:G	**158**	1	Liu 2005	x	
BaP	**CGC**	**CTC**	**G:C>T:A**	**158**	**1**	Liu 2005	x	x
BaP	GAA	TAA	G:C>T:A	198	1	Unpublished		
BaP	GTG	TTG	G:C>T:A	216	1	Reinbold 2007		
BaP	GAG	GAA	G:C>A:T	**224**	1	Liu 2005	x	
BaP	CGG	CCG	G:C>C:G	**248**	1	Reinbold 2007	x	
BaP	**CGT**	**GGT**	**G:C>C:G**	**273**	**1**	Reinbold 2007	x	x
BaP	**CGT**	**TGT**	**G:C>A:T**	**273**	**1**	Reinbold 2007	x	x
BaP	CGT	CAT	G:C>A:T	**273**	1	Liu 2005	x	
BaP	CGT	CTT	G:C>T:A	**273**	2	Reinbold 2007	x	
BaP	CCT	TCT	G:C>A:T	278	1	Liu 2005		
BaP	GGG	TGG	G:C>T:A	279	1	Liu 2005		
BaP	AGA	GGA	A:T>G:C	280	1	Liu 2005		
BaP	GAC	GAA	G:C>T:A	281	1	Reinbold 2007		
BaP	CGG	CTG	G:C>T:A	**282**	1	Reinbold 2007	x	
AAI	ACT	TCT	A:T>T:A	55	1	Nedelko 2009		
AAI	CAG	CTG	A:T>T:A	104	1	Nedelko 2009		
AAI	CTC	CAC	A:T>T:A	130	1	Feldmeyer 2006		
AAI	AAC	TAC	A:T>T:A	**131**	1	Nedelko 2009	x	
AAI	AAC	ATC	A:T>T:A	**131**	1	Nedelko 2009	x	
AAI	**TGC**	**TGG**	**G:C>C:G**	**135**	**3**	Nedelko 2009	x	x
AAI	AAG	TAG	A:T>T:A	139	1	Feldmeyer 2006		
AAI	**GGC**	**GTC**	**G:C>T:A**	**154**	**1**	Nedelko 2009	x	x
AAI	CGC	GGC	G:C>C:G	**158**	1	Liu 2004	x	
AAI	GCC	CCC	G:C>C:G	159	1	Nedelko 2009		
AAI	AAG	TAG	A:T>T:A	164	1	Nedelko 2009		
AAI	CAC	CAG	G:C>C:G	168	1	Nedelko 2009		
AAI	ATG	TTG	A:T>T:A	169	1	Nedelko 2009		
AAI	TGC	TGG	G:C>C:G	176	1	Liu 2004		
AAI	CAT	CGT	A:T>G:C	179	1	Nedelko 2009		
AAI	CAT	CTT	A:T>T:A	193	1	Feldmeyer 2006		
AAI	CTT	TTT	G:C>A:T	194	1	Nedelko 2009		
AAI	GTG	GTC	G:C>C:G	**203**	1	Feldmeyer 2006	x	
AAI	AGA	TGA	A:T>T:A	209	3	Liu 2004, Nedelko 2009		
AAI	CGA	CCA	G:C>C:G	**213**	1	Nedelko 2009	x	
AAI	AAC	GAC	A:T>G:C	239	1	Nedelko 2009		
AAI	GGC	GCC	G:C>C:G	**245**	1	Nedelko 2009	x	
AAI	AGG	TGG	A:T>T:A	**249**	2	Nedelko 2009	x	
AAI	GAA	GAC	A:T>C:G	258	1	Nedelko 2009		

Table S5 continued.

Treatment	WT codon	Mutant codon	Base change	Codon	Occurrence: HUF cell lines	Reference	Codon mutated in current study	Mutation match with current study
AAI	CGT	TGT	G:C>A:T	**273**	1	Nedelko 2009	x	
AAI	AGA	AGT	A:T>T:A	280	1	Liu 2004		
AAI	GAC	GTC	A:T>T:A	281	1	Liu 2004		
AAI	GAA	GTA	A:T>T:A	**286**	1	Feldmeyer 2006	x	
AAI	AAG	TAG	A:T>T:A	291	1	Nedelko 2009		
AAI	AAG	TAG	A:T>T:A	305	1	Nedelko 2009		
AAI	AGC	TGC	A:T>T:A	313	1	Feldmeyer 2006		
UV	**TGC**	**TGG**	**G:C>C:G**	**135**	**1**	Liu 2004	x	x
UV	CCC	TCC	G:C>A:T	151	1	Liu 2004		
UV	CAT	TAT	G:C>A:T	179	1	Liu 2004		
UV	**CGG**	**CAG**	**G:C>A:T**	**248**	**1**	Liu 2004	x	x
UV	AGG	AGA	G:C>A:T	**249**	1	Liu 2004	x	
UV	CCC	CAC	G:C>T:A	250	1	Liu 2004		
UV	CAG	TAG	G:C>A:T	317	1	Liu 2004		
MNNG	TCC	TTC	C to T	99	1	Nedelko 2009		
MNNG	TTC	GTC	T to G	113	1	Nedelko 2009		
MNNG	TGC	TAC	G to A	141	1	Nedelko 2009		
MNNG	CCG	TCG	C to T	152	1	Nedelko 2009		
MNNG	GCC	GTC	C to T	159	1	Nedelko 2009		
MNNG	CAG	TAG	C to T	165	1	Nedelko 2009		
MNNG	TCC	TTC	C to T	241	1	Nedelko 2009		
MNNG	TCC	TTC	C to T	241	1	Nedelko 2009		
MNNG	GGC	GAC	G to A	**245**	1	Nedelko 2009	x	
MNNG	**GTG**	**ATG**	**G to A**	**272**	**1**	Nedelko 2009	x	x
MNNG	GAC	GAG	C to G	281	1	Nedelko 2009		
MNNG	CGG	TGG	C to T	**282**	1	Nedelko 2009	x	
MNNG	AAA	TAA	A to T	321	1	Nedelko 2009		
control	GGC	GCC	G:C>C:G	105	1	Whibley 2010		
control	TTC	GTC	A:T>C:G	113	2	Whibley 2010		
control	AAG	ACG	A:T>C:G	120	1	Whibley 2010		
control	AAG	ACG	A:T>C:G	**132**	1	Whibley 2010	x	
control	TTT	GTT	A:T>C:G	134	2	Whibley 2010		
control	**TGC**	**TGG**	**G:C>C:G**	**135**	**7**	Whibley 2010	x	x
control	GCC	CCC	G:C>C:G	138	2	Whibley 2010		
control	AAG	AAC	G:C>C:G	139	1	Whibley 2010		
control	**GTG**	**ATG**	**G:C>A:T**	**143**	**1**	Whibley 2010	x	x
control	GTT	GGT	A:T>C:G	147	3	Whibley 2010		
control	GCC	CCC	G:C>C:G	159	1	Whibley 2010		
control	GCC	GGC	G:C>C:G	161	1	Whibley 2010		
control	GCC	CCC	G:C>C:G	161	1	Whibley 2010		
control	GTG	ATG	G:C>A:T	173	1	Whibley 2010		
control	CGC	CAC	G:C>A:T	175	1	Whibley 2010		
control	TGC	TGG	G:C>C:G	176	2	Whibley 2010		
control	TGC	TAC	G:C>A:T	176	1	Whibley 2010		
control	TGC	TTC	G:C>T:A	176	1	Whibley 2010		
control	CAT	TAT	G:C>A:T	179	1	Whibley 2010		
control	CTT	TTT	G:C>A:T	194	1	Whibley 2010		
control	ATC	ACC	A:T>G:C	**195**	1	Whibley 2010	x	
control	GTG	CTG	G:C>C:G	216	1	Whibley 2010		
control	AAC	AGC	A:T>G:C	239	1	Whibley 2010		
control	AGT	AGG	A:T>C:G	240	1	Whibley 2010		
control	GGC	GAC	G:C>A:T	**245**	2	Whibley 2010	x	
control	GGC	GCC	G:C>C:G	**245**	5	Whibley 2010	x	
control	ATG	AAG	A:T>T:A	246	1	Whibley 2010		
control	**AGG**	**AGC**	**G:C>C:G**	**249**	**2**	Whibley 2010	x	x
control	ATC	AGC	A:T>C:G	255	2	Whibley 2010		
control	GAA	GAC	A:T>C:G	258	1	Whibley 2010		
control	CTG	CCG	A:T>G:C	**265**	1	Whibley 2010	x	
control	**CGT**	**GGT**	**G:C>C:G**	**273**	**2**	Whibley 2010	x	x
control	CGT	TGT	G:C>A:T	**273**	2	Whibley 2010	x	
control	**TGT**	**TTT**	**G:C>T:A**	**275**	**1**	Whibley 2010	x	x
control	GCC	GGC	G:C>C:G	276	1	Whibley 2010		
control	AGA	ACA	G:C>C:G	280	1	Whibley 2010		
control	GAC	GAG	G:C>C:G	281	3	Whibley 2010		
control	GAC	AAC	G:C>A:T	281	1	Whibley 2010		
control	GAC	CAC	G:C>C:G	281	2	Whibley 2010		

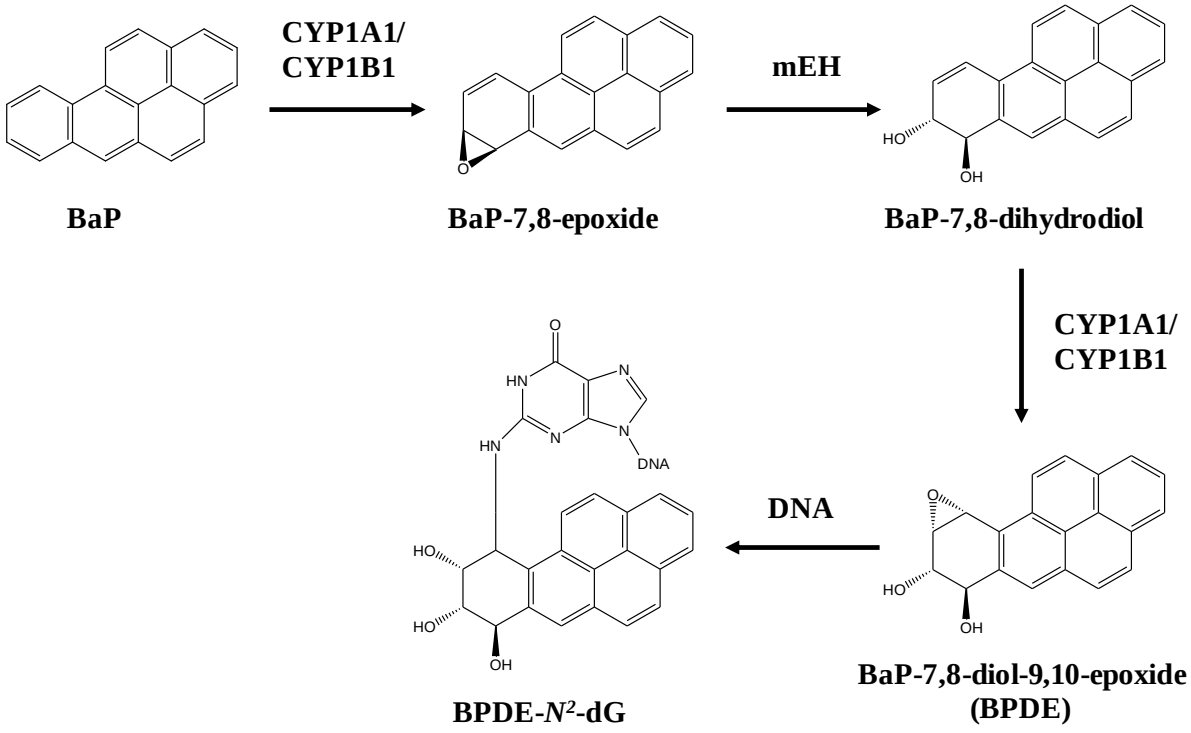

Figure S1. Metabolic activation of BaP to the reactive intermediate BPDE and subsequent DNA adduct formation. BaP is first oxidised by CYP1A1 and CYP1B1 to form BaP-7,8-epoxide, which is then converted to BaP-7,8-dihydrodiol by mEH. Further oxidation by CYP1A1/CYP1B1 leads to the formation of the ultimate reactive species, BPDE. BPDE preferentially reacts with guanine residues in DNA, and the 10-(deoxyguanosin-N^2-yl)7,8,9-trihydroxy-7,8,9,10-tetrahydro-BaP (BPDE-N^2-dG) adduct is the major adduct formed by BPDE both *in vitro* and *in vivo*. CYP, cytochrome P450; mEH, microsomal epoxide hydrolase.

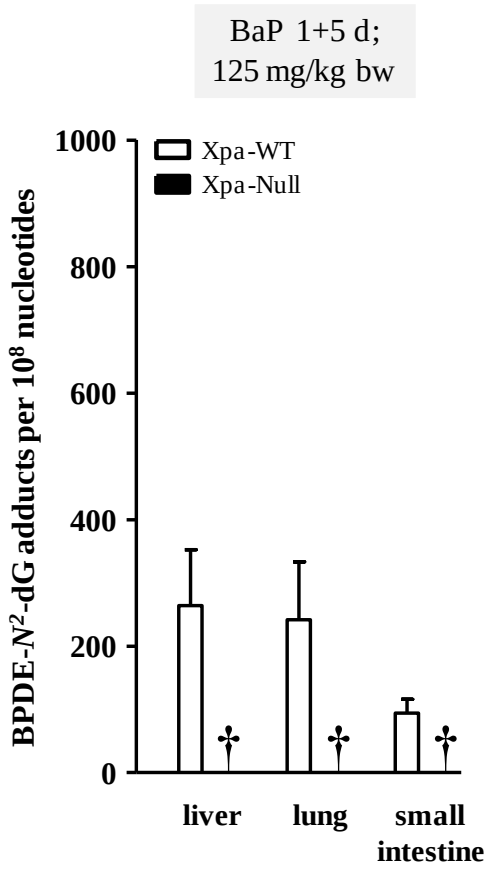

Figure S2. BPDE-N^2-dG adduct levels in Xpa-WT and Xpa-Null Hupki mice assessed 5 days after a single treatment with BaP. Mice were treated with 125 mg/kg bw BaP and DNA adduct levels in different tissues were assessed by ^{32}P-postlabelling. Values represent means ± SD from 3 animals, and each DNA sample was measured by two independent ^{32}P-postlabelling analyses. † = not determined due to death of Xpa-Null animals.

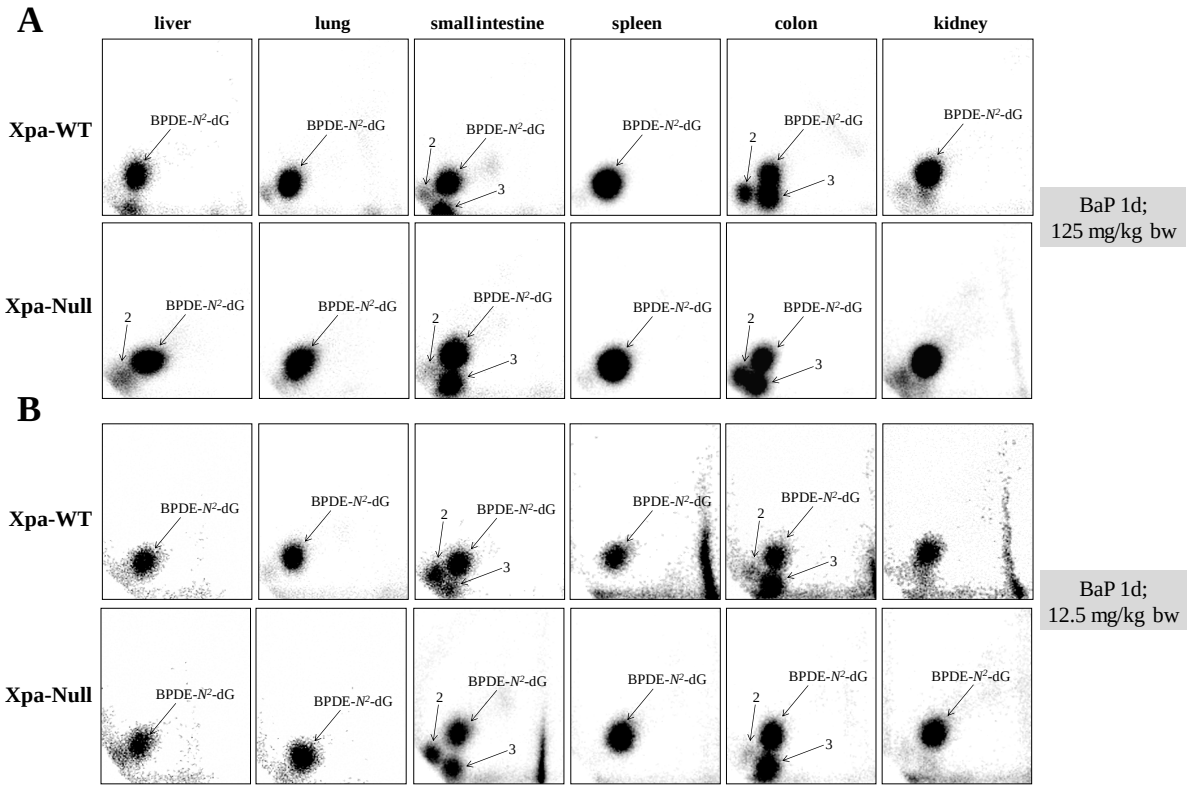

Figure S3. DNA adduct pattern induced in Xpa-WT and Xpa-Null Hupki mice treated with BaP. Autoradiographic profiles of DNA adducts obtained in mice treated with (A) 125 or (B) 12.5 mg/kg bw BaP, as indicated, and adducts in different tissues were detected by ^{32}P-postlabelling; the origins, in the bottom left-hand corner, were cut off before exposure. The major DNA adduct detected in all tissues examined was previously identified as 10-(deoxyguanosin-N^2-yl)-7,8,9-trihydroxy-7,8,9,10-tetrahydrobenzo[*a*]pyrene (BPDE-N^2-dG) [1]. Adduct spot 2 was previously suggested to be derived from reaction of 9-hydroxy-BaP-4,5-epoxide with guanine [2]. Adduct spot 3 has not yet been structurally identified.

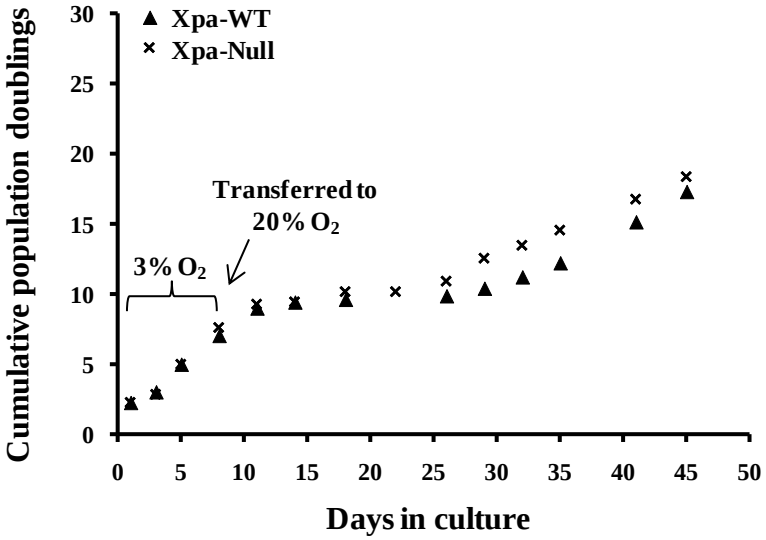

Figure S4. Growth of HUFs at 20% O_2 following one week of culture at 3% O_2. Xpa-WT and Xpa-Null primary HUFs (2.5×10^5 cells/ 25-cm^2 flask) were cultured for one week at 3% O_2 and then transferred to 20% O_2 for a further five weeks of culture. Cells were counted every 3–4 days, diluted and reseeded to determine the cumulative population doublings over time.

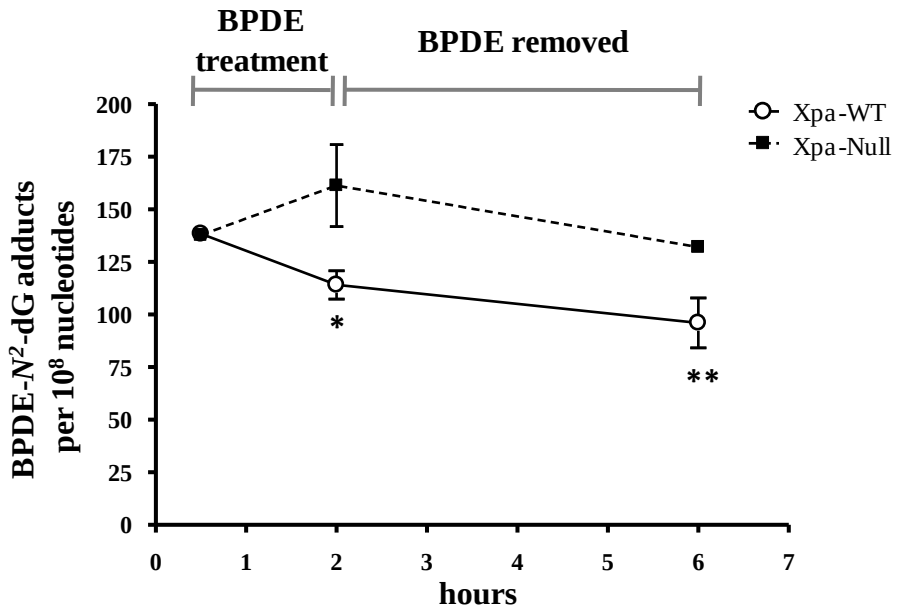

Figure S5. BPDE-DNA adduct repair in Xpa-WT and Xpa-Null HUFs. HUFs were exposed to 0.25 μM BPDE for up to 2 hr. Treated cells were harvested following 0.5 hr and 2 hr of exposure, or BPDE was removed and replaced with normal growth medium. In the latter case, cells were cultured for an additional 4 hr, and then harvested. Harvested cells were assessed for BPDE-N^2-dG adduct formation by ^{32}P-postlabelling. Values represent means ± SD of two separate experiments where each DNA sample was measured by two independent ^{32}P-postlabelling analyses. Statistical analysis, comparing DNA adduct levels in Xpa-WT and Xpa-Null HUFs, was performed by 2-factor ANOVA followed by Bonferroni's post-hoc contrasts; * $P < 0.05$, ** $P < 0.01$.

References for Supplementary Material

[1] V.M. Arlt, M. Stiborova, C.J. Henderson, M. Thiemann, E. Frei, D. Aimova, R. Singh, G. Gamboa da Costa, O.J. Schmitz, P.B. Farmer, C.R. Wolf, D.H. Phillips, Metabolic activation of benzo[a]pyrene in vitro by hepatic cytochrome P450 contrasts with detoxification in vivo: experiments with hepatic cytochrome P450 reductase null mice, Carcinogenesis, 29 (2008) 656-665.

[2] M. Stiborova, M. Moserova, V. Cerna, R. Indra, M. Dracinsky, M. Sulc, C.J. Henderson, C.R. Wolf, H.H. Schmeiser, D.H. Phillips, E. Frei, V.M. Arlt, Cytochrome b5 and epoxide hydrolase contribute to benzo[a]pyrene-DNA adduct formation catalyzed by cytochrome P450 1A1 under low NADPH:P450 oxidoreductase conditions, Toxicology, 318 (2014) 1-12.

[3] D.M. DeMarini, S. Landi, D. Tian, N.M. Hanley, X. Li, F. Hu, B.C. Roop, M.J. Mass, P. Keohavong, W. Gao, M. Olivier, P. Hainaut, J.L. Mumford, Lung tumor KRAS and TP53 mutations in nonsmokers reflect exposure to PAH-rich coal combustion emissions, Cancer Res, 61 (2001) 6679-6681.

[4] F.H. Sarkar, Y. Li, V. Vallyathan, Molecular analysis of p53 and K-ras in lung carcinomas of coal miners, International journal of molecular medicine, 8 (2001) 453- 459.

[5] J. vom Brocke, A. Krais, C. Whibley, M.C. Hollstein, H.H. Schmeiser, The carcinogenic air pollutant 3-nitrobenzanthrone induces GC to TA transversion mutations in human p53 sequences, Mutagenesis, 24 (2009) 17-23.

[6] Z. Liu, K.R. Muehlbauer, H.H. Schmeiser, M. Hergenhahn, D. Belharazem, M.C. Hollstein, p53 mutations in benzo(a)pyrene-exposed human p53 knock-in murine fibroblasts correlate with p53 mutations in human lung tumors, Cancer Res, 65 (2005) 2583-2587.

[7] M. Reinbold, J.L. Luo, T. Nedelko, B. Jerchow, M.E. Murphy, C. Whibley, Q. Wei, M. Hollstein, Common tumour p53 mutations in immortalized cells from Hupki mice heterozygous at codon 72, Oncogene, 27 (2008) 2788-2794.

[8] T. Nedelko, V.M. Arlt, D.H. Phillips, M. Hollstein, TP53 mutation signature supports involvement of aristolochic acid in the aetiology of endemic nephropathy-associated tumours, Int J Cancer, 124 (2009) 987-990.

[9] N. Feldmeyer, H.H. Schmeiser, K.R. Muehlbauer, D. Belharazem, Y. Knyazev, T. Nedelko, M. Hollstein, Further studies with a cell immortalization assay to investigate the mutation signature of aristolochic acid in human p53 sequences, Mutat Res, 608 (2006) 163-168.

[10] Z. Liu, M. Hergenhahn, H.H. Schmeiser, G.N. Wogan, A. Hong, M. Hollstein, Human tumor p53 mutations are selected for in mouse embryonic fibroblasts harboring a humanized p53 gene, Proc Natl Acad Sci U S A, 101 (2004) 2963-2968.

[11] C. Whibley, A.F. Odell, T. Nedelko, G. Balaburski, M. Murphy, Z. Liu, L. Stevens, J.H. Walker, M. Routledge, M. Hollstein, Wild-type and Hupki (human p53 knock-in) murine embryonic fibroblasts: p53/ARF pathway disruption in spontaneous escape from senescence, J Biol Chem, 285 (2010) 11326-11335.